Laboratory and numerical experiments on stem waves due to monochromatic waves along a vertical wall

Sung Bum Yoon[1], Jong-In Lee[2], Young-Take Kim[3] and Choong Hun Shin[1]

[1]Department of Civil and Environmental Engineering, Hanyang University, EIRCA Campus, Ansan, Gyeonggi, 15588, South Korea
[2]Department of Marine and Civil Engineering, Chonnam National University, Yeosu Campus, Yeosu, Jeonnam, 59626, South Korea
[3]River and Coastal Research Division, Korea Institute of Civil Engineering & Building Technology, Goyang, Gyeonggi, 10223, South Korea

Correspondence to: Choong Hun Shin (lavici@hanyang.ac.kr)

Abstract. In this study, both laboratory and numerical experiments are conducted to investigate stem waves propagating along a vertical wall developed by the incidence of monochromatic waves. The results show the following features: For small amplitude waves, the wave heights along the wall show a slowly varying undulation. Normalized wave heights perpendicular to the wall show a standing wave pattern. Thus, overall wave pattern in the case of small amplitude waves show a typical diffraction pattern around a semi-infinite thin breakwater. As the amplitude of incident waves increases, both the undulation intensity and the asymptotic normalized wave height decrease along the wall. For larger amplitude waves with smaller angle of incidence, the measured data show clearly stem waves. Numerical simulation results are in good agreement with the results of laboratory experiments. It is found from a simple geometric relationship of wave pattern that the lengthening of wave length due to the nonlinearity of waves is responsible for the development of stem waves along the wall. The results of present experiments support favorably the existence and the properties of stem waves found by other researchers using numerical simulations.

1 Introduction

Coastal structures have been increasingly constructed in deep water regions as the size of ships becomes larger. In such deep water regions, a vertical-type structure is preferred to save construction costs. In the case of a vertical structure, stem waves occur when waves propagate obliquely against the structure. Thus, there is a need for careful consideration to secure appropriate free board and stability of caisson blocks.

Based on laboratory experiments on the reflection of a solitary wave propagating obliquely against a vertical wall, Perroud (1957) reported the existence of three types of waves when the angle between incident wave ray and a vertical wall is below 45°: incident, reflected, and stem waves. Berger and Kohlhase (1976) conducted laboratory experiments and found that stem waves appeared also in the case of sinusoidal waves, and that the properties of stem waves developed by sinusoidal waves showed similarities to those of solitary waves. On the other hand, according to laboratory experiments by Melville (1980)

with solitary waves, the width and height of stem waves were found to be wider and larger, respectively, as waves propagated along the wall. However, the wave height did not exceed double the height of incident waves. Yue and Mei (1980) analysed stem waves at a constant water depth using parabolic approximation equations for second-order Stokes waves. They found that the influence of reflected waves was removed when the incident angle between the structure and the waves was below 20° and that only incident waves and stem waves appeared. Liu and Yoon (1986) showed that stem waves occurred also in an area along the line of a depth discontinuity, as in the case of a vertical wall. In addition, Yoon and Liu (1989) introduced a parabolic approximation equation based on the Boussinesq equation and analysed stem waves for the case of cnoidal incident waves. Yoon and Liu (1989) showed the importance of the incident wave nonlinearity. Most previous studies on stem waves focused on the properties of stem waves depending on incident angle and wave nonlinearity of monochromatic waves.

The real-sea wave conditions, however, show the nature of random waves. Mase et al. (2002) performed both laboratory experiments and numerical simulations on stem waves along a vertical wall for the case of unidirectional random waves, and investigated changes of stem wave characteristics associated with incident wave conditions. The numerical model employed by Mase et al. (2002) was a nonlinear parabolic approximation equation model based on the so-called spectral KP (Kadomtsev and Petviashvili, 1970) equation extended to deep water. By comparing measured and calculated wave heights along the wall with the linear diffraction solution of the Sommerfeld theory (Sommerfeld, 1896), Mase et al. (2002) showed that measured wave heights along a wall decreased much faster after reaching a peak than those predicted by the nonlinear numerical model or the linear diffraction solution. The reason for this was not clarified by the authors. The comparison between results from hydraulic and numerical experiments does not give favorable agreement. Moreover, the measured wave height distribution normal to the wall was not presented for the cases of constant water depth.

Even though the existence and the properties of stem waves for sinusoidal waves are well known theoretically via numerical simulations (e.g., Yue and Mei, 1980; Yoon and Liu, 1989), they are not yet fully supported by physical experiments. Berger and Kohlhase (1976) and Mase et al. (2002) conducted hydraulic experiments to show the existence of stem waves for the cases of sinusoidal waves. Their experimental data, however, failed to produce clear stem waves, possibly due to partial reflection from the beach, diffraction from the ends of vertical wall, or insufficient space in the wave basin. Lee et al. (2003), Lee and Yoon (2006) and Lee and Kim (2007) performed laboratory experiments to investigate stem waves for sinusoidal waves, and compared the measured waves with the numerical results obtained using a nonlinear parabolic approximation equation model. Their hydraulic experiments demonstrated stem waves for some cases with a relatively large incident wave. However, the stem waves were not clearly developed because of both the narrowness of wave basin and the reflected waves from the beach. Only four cases of incident wave conditions were tested in their experiment. Thus, the experimental data were not sufficient to investigate the properties of stem waves. Moreover, the numerical results for the cases of large angle of incidence were not highly accurate because of the small-angle parabolic model employed for their numerical simulations. Thus, there is still need to perform a precisely controlled experiment to investigate the existence and the properties of stem waves. In this study, precisely-controlled laboratory experiments are conducted to investigate the characteristics of stem

waves developed by the incidence of monochromatic waves. The measured data are compared with numerical simulations and analytical solutions. In the following section, the numerical simulation and the analytical solution employed in this study are summarized. In section 3, the experimental setup and procedure are briefly presented. In section 4, the measured wave heights are compared with numerically simulated results and analytical solutions. This section also discusses the effects of both nonlinearity and angle of incidence. In the final section, the major findings from this study are summarized.

2 Numerical simulation and analytical solution

In this study, the stem waves developed along a vertical wall over a constant water depth are investigated for the cases of monochromatic waves. Fig. 1 shows the definition sketch of the wave field around a vertical wedge. The monochromatic waves are symmetrically incident towards the tip of the wedge. The *x*-axis of the coordinate system is aligned with a side wall of the wedge. The angle of incidence θ_0 is defined as the angle between the x-axis and the incident wave ray. The computational domain lies in the region of $0 \leq$ x and y ≤ 0.

2.1 Numerical simulation

In this study, the latest version of REF/DIF, a wide-angle nonlinear parabolic approximation equation model developed by Kirby et al (2002), is employed to simulate stem waves. This numerical model can deal with both amplitude and frequency dispersions of waves. In this study, the water depth is uniform, and no ambient current is present. Thus, the governing equation of the REF/DIF model is simplified as:

$$2ik\frac{\partial A}{\partial x}+\frac{\partial^2 A}{\partial y^2}+\frac{i}{2k}\frac{\partial^3 A}{\partial x \partial y^2}-\frac{\omega k^3}{C_g}D|A|^2A=0 \tag{1}$$

where h is the water depth, $i=\sqrt{-1}$, C_g is the wave group velocity, A is the complex wave amplitude, k and ω are the wave number and the angular frequency, respectively, and satisfy the following linear dispersion relationship:

$$\omega^2 = gk\tanh kh \tag{2}$$

where g is the gravitational acceleration, and D is given as:

$$D=\frac{\cosh 4kh+8-2\tanh^2 kh}{8\sinh^4 kh} \tag{3}$$

The third term of Eq. (1) is the correction term for the wide angle parabolic approximation. The conventional parabolic approximation equation, i.e., the nonlinear Schrödinger equation of Yue and Mei (1980) is obtained if this term is neglected. The last term represents the nonlinear effect of waves. Fig. 2 shows the coordinate system for the present numerical simulation in comparison with that of Yue and Mei (1980). In the present simulation the incident waves are prescribed obliquely along the *y*-axis as:

$$A = A_0 e^{ik_n y \sin\theta_0} \tag{4}$$

where A_0 is the amplitude of the incident wave, and k_n is the nonlinear wave number given as:

$$k_n = k\left(1 - \frac{C}{2C_g} D(k|A|)^2\right) \tag{5}$$

where $C(=\omega/k)$ is the phase speed of wave. No-flux boundary condition is prescribed along the vertical wall (y = 0) given as:

$$\frac{\partial A}{\partial y} = 0 \tag{6}$$

In the numerical model of Yue and Mei (1980) the waves are incident normal to the *y*-axis. Thus, the uniform waves are prescribed along the y-axis as:

$$A = A_0 \tag{7}$$

Along the vertical wall ($y = -x\tan\theta_0$) the no-flux boundary condition is given as:

$$\frac{\partial A}{\partial y} = ikA_0 \tan\theta_0 \tag{8}$$

Since this boundary condition uses the linear version of wave number, the accuracy of the solution decreases when the wave height of incident wave increases. For the later use the nonlinear parameter, K, proposed by Yue and Mei (1980) is given as:

$$K = \left(\frac{kA_0}{\tan\theta_0}\right)^2 \frac{C}{C_g} \frac{\cosh 4kh + 8 - 2\tanh^2 kh}{8\sinh^4 kh} \tag{9}$$

K is the single parameter representing both the nonlinearity of incident wave and the angle of incidence on the formation of stem waves along the vertical wall.

2.2 Analytical solution

Chen (1987) developed an analytical solution for the combined reflection and diffraction of monochromatic waves due to a vertical wedge. The analytical solution is given in a polar coordinate as shown in Fig. 1 as:

$$\Phi(r,\theta^*,z,t) = -\frac{igA}{\omega}\frac{\cosh\{k(z+h)\}}{\cosh kh}F(r,\theta^*)e^{i\omega t} \tag{10}$$

where $\Phi(r,\theta^*,z,t)$ is the velocity potential, and $F(r,\ \theta^*)$ is a diffraction factor given as:

$$F(r,\theta^*) = \frac{2}{\nu}\left[J_0(kr) + 2\sum_{n=1}^{\infty} e^{in\pi/2\nu}J_{n/\nu}(kr)\cos\frac{n\alpha^*}{\nu}\cos\frac{n\theta^*}{\nu}\right] \tag{11}$$

where $\theta^* = \theta - 2\theta_0$, $\alpha^* = \pi - \theta_0$, $\nu = 2(\pi - \theta_0)/\pi$, and θ_0 is the angle of incidence. $J_0(kr)$ is the Bessel function of the first kind of order 0. The absolute value of the diffraction factor $|F(r,\theta^*)|$ represents the normalized wave height H/H_0 where H_0 is the wave height of the incident wave. The analytical solution of Chen (1987) is linear. Thus, when the wave height of incident waves is not small, the accuracy of the solution decreases.

3 Hydraulic experiments

Hydraulic experiments are carried out in the multidirectional irregular wave generation basin of the Korea Institute of Construction Technology (see Photo 1). The basin used in the laboratory experiments is 42 m long, 36 m wide and 1.05 m high. A snake-type wave generator consisting of 60 wave boards, each with dimensions of 0.5 m in width and 1.1 m in height and driven by an electronic servo piston, is installed along the 36 m long bottom wall of the wave basin. Free surface displacements are measured using 0.6 m long capacitance-type wave gauges with the measuring range of ±0.3 m.

Fig. 3 shows the configuration of the experimental setup and model installation. A 30 m long vertical wall is installed along the left lateral side of the basin in four different orientations. A dissipating gravel beach with a 1/20 slope is arranged on the opposite side of the wave generator to reduce the reflection of waves inside the basin. Another dissipating beach and wave absorber are also set along the lateral sides and at the back of the wave generator. Along the lateral side opposite to the vertical wall a 10 m long wave guide is installed to avoid diffraction from the side wall. Note that θ_0 is the angle between the vertical wall and the incident waves. The origin of the spatial coordinate system of the laboratory experiments (i.e., x_0, y_0) is

set at the tip of the vertical wall which is located 3 m and 5 m away from the lateral side and the wave generator, respectively, as shown in Fig. 3. The width and height of the vertical wall were both 0.6 m. The experiments are carried out at a constant water depth of h = 0.25 m. The free board from a still water level to the top of the vertical wall is 0.35 m in order to prevent overtopping of waves.

The incident wave conditions are summarized in Table 1. The title of each test case is composed of three alphabet characters and a numeric digit. The first alphabet M stands for 'monochromatic' waves. The second alphabet S or L represents 'shorter' or 'longer' waves in terms of period, respectively. The third alphabet S, M or L represents 'small', 'medium', or 'large' waves in terms of wave height, respectively. Finally, the numeric digit represents the size of the angle of incidence.

The wave periods of T = 0.7 s and 1.1 s are tested. The wave heights are H_0 = 0.009 m, 0.027 m, and 0.036 m for 0.7 s waves, and H_0 = 0.018 m, 0.054 m, and 0.072 m for 1.1 s waves so that no wave breaking occurs during the experiments. The length of the vertical wall in the laboratory experiments is 40L for the case of T = 0.7 s and 20L for the case of T = 1.1 s, where L represents the wavelength of monochromatic waves corresponding to the given period T. The incident angles of θ_0=10°, 20°, 30°, and 40° are obtained by adjusting the orientation of the vertical wall. Thus, the incident waves propagate normal to the line of the wave generator. The nonlinearity of the incident waves are presented in two dimensionless parameters, wave steepness kH_0 and the nonlinear parameter K given by Eq. (9).

In the experiments, wave heights are measured along both the vertical wall (x-direction) and normal to the vertical wall (y-direction). Note that wave heights in the x-direction are measured 0.05 m away from the front side of the wall, while wave heights in the y-direction are measured along two lines of x = 6L and 15L. The intervals of the wave height measurement positions are $\Delta x = 0.2$ m and 0.4 m for $T = 0.7$ s and 1.1 s, respectively, along the wall, while $\Delta y =$ 0.1 m and 0.2 m for $T = 0.7$ s and 1.1 s, respectively, normal to the wall. Table 2 gives a summary of the wave height measurement positions. The wave heights are extracted from the measured free surface displacements using the zero-up-crossing method. Photo 2 shows the hexagonal or beehive wave pattern captured during the experiment in front of a vertical wall for the case of $\theta_0 = 30°$. This is typical of the cross-sea generated by the oblique interaction of two or more traveling plane waves (see e.g., Le Mehauté, 1976; Mei, 1983; Nicholls, 2001). Postacchini et al. (2014) studied the generation and evolution of large-scale eddies of vertical axis generated by the breaking of two crossing wave trains.

Prior to the main experiments the performance of the wave generator is tested. For this test no vertical wall is placed in the wave basin. After the initiation of wave generation the time histories of free surface displacement are recorded at three incident-wave-measuring points as shown in Fig. 3. The first part of data with a sufficiently long time is discarded, and the wave height and period are obtained using the zero-up-crossing method. The tests show that the target waves are well generated, and also showed that the bottom friction is negligible within the test area of the wave basin. In particular, three wave gauges aligned in a wave propagation direction with a specified distance are placed at the incident-wave-measuring point located near the gravel beach with a 1/20 slope to estimate the wave reflection from the beach. The incident and reflected waves are separated using the three-point higher order separation technique. This higher order technique is developed for finite amplitude waves by adding the second and third harmonics to the linear separation scheme proposed by

Suh et al. (2001). The reflection coefficient due to the gravel beach is maintained at less than 3% for all the waves considered in the experiments.

4 Results and discussions

In this study, experiments on the formation of stem waves around a vertical wall are conducted and the measured wave heights are compared with results calculated using both the wide-angle parabolic approximation equation numerical model, REF/DIF, and the analytical solution of Chen (1987).

4.1 Shorter waves (T = 0.7 s)

Fig. 4 shows the comparisons between the measured, numerically simulated, and analytically calculated wave heights, H/H_0, along the vertical wall for the cases of H_0 = 0.009 m with T = 0.7 s (i.e., MSS-series). The amplitude of the incident waves is small as the title of the test cases indicates. The solid circles represent the results of the laboratory experiments. The solid and dashed lines represent the numerical (using REF/DIF) and analytical solution results, respectively. Various incident angles of θ_0=10°, 20°, 30°, and 40° are presented. For the case of small angle of incidence (MSS1, θ_0=10°) the measured wave height along the vertical wall increases monotonically with the distance from the tip of the vertical wall. As the angle of incidence increases, the wave height shows a slowly varying undulation with the average value of $H/H_0 = 2.0$. The maximum value of undulation is approximately $H/H_0 \approx 2.3$, and the location of maximum wave height decreases with increasing angle of incidence. In particular, the overall pattern of wave height distribution does not support the generation of stem waves, which are characterized by uniform wave heights smaller than those obtained from linear diffraction theory (Yue and Mei, 1980; Yoon and Liu, 1989). The wave heights calculated using the REF/DIF numerical model (Kirby and Dalrymple, 1994) and the analytical solution of Chen (1987) agree well with the measured wave heights. This supports the idea that the effects of nonlinearity of incident waves are too weak to develop stem waves. In the case of $\theta_0 = 10°$, the maximum normalized wave heights does not reach $H/H_0 \approx 2.3$ because the size of the experimental area is insufficient. If the vertical wall is sufficiently long, the same result may also be obtained for $\theta_0 = 10°$.

Figs. 5 and 6 show the comparisons of wave heights H/H_0 along a line (x = 6L, 15L) perpendicular to the vertical wall. The distribution of wave height shows the typical pattern of standing waves formed by superposition of the reflected waves on the incident waves. Berger and Kohlhase (1976) called these standing waves as stem waves as long as they propagated parallel to the wall. If stem waves, however, are defined as waves with a uniform wave height in the direction normal to the wall, then the wave height distributions for these small amplitude waves in MSS-series show no sign of stem waves. The wave amplitude for this MSS-series is too small to generate stem waves along the wall.

Fig. 7 shows normalized wave heights along the vertical wall for the cases of MSM-series (i.e., H_0 = 0.027 m, T = 0.7 s) with various angles of incidence. The amplitude of the incident waves is three times larger than the MSS-series waves. Figs. 8 and 9 show normalized wave heights perpendicular to the vertical wall at positions x = 6L and 15L, respectively. The results

shown in Fig. 7 indicate that, when the angle of incidence is small ($\theta_0 = 10°$), the normalized wave height approaches to a uniform value of $H/H_0 \approx 1.75$ as waves propagated along the vertical wall. At larger incident angles, the maximum normalized wave heights reach up to $H/H_0 \approx 2.25$, and showed a slowly varying undulation.

In the results shown in Figs. 8 and 9 the stem waves of uniform wave height are found under the conditions of $\theta_0 = 10°$ and $x = 15L$, albeit the stem width is small. However, in the cases of other incident angles, stem waves do not appear. The red lines shown in the figure represent the stem waves. The definition of stem width is rather controversial. Yue and Mei (1980) defined the stem width as the distance from the wall to the edge of the uniform wave amplitude region in the direction of incident wave crest lines. However, it is not an easy task to locate the edge of the flat region. On the other hand, Berger and Kohlhase (1976) defined the stem width as the distance along the stem crest lines from the wall to the first nodal line of standing wave pattern which is easier to identify from the measured data. In this study the stem edge was determined as a point which is apart from the first nodal point towards the wall by a distance λ between the first node and the second antinode (see Figs. 8 and 9). This new definition of stem width is easier to determine and is consistent with the definition of Yue and Mei (1980).

The results from laboratory experiments are in good agreement with those of the results of REF/DIF model. However, the analytical solutions of Chen (1987) do not agree well with the measured data, probably because of nonlinear interactions between incident and reflected waves. The discrepancy between the analytical solution of Chen (1987) and the measured data decreases as the angle of incidence increases. This can be attributed to the decrease in the intensity of nonlinear interactions between incident and reflected waves as the angle of incidence increases.

Figs. 10, 11, and 12 show the comparisons of the measured, numerically simulated, and analytically calculated results for the cases of MSL-series (H_0 = 0.036 m, T = 0.7 s). The amplitude of the incident waves is the largest among the shorter wave test cases. For the cases of smaller angle of incidence, $\theta_0 = 10°$ and $20°$, the normalized wave height increases monotonically to reach a constant value of $H/H_0 \approx 1.5$ and 2.1, respectively, with a strong indication of stem wave development. In the cases of larger angle of incidence the wave heights show a slowly varying undulation. As shown in Figs. 11 and 12, which represent normalized wave heights in the direction normal to the vertical wall, stem waves appear clearly for $\theta_0 = 10°$ along x = 6L and 15L. It can also be seen that the width of stem waves increases in proportion to the distance from the tip of vertical wall. For the case of the angle of incidence, $\theta_0 = 20°$, stem waves are also developed along the line of x = 15L, but are much weaker than the small angle case. In the cases of larger incidence angles, the normalized wave heights tend to show a distribution pattern similar to that of standing waves normal to the wall.

4.2 Longer waves (T = 1.1 s)

Figs. 13, 14 and 15 show comparisons between the measured, numerically simulated, and analytically calculated wave heights H/H_0 along the vertical wall (y=0) and normal to the wall (x = 6L and 15L) for the cases of H_0 = 0.018 m with T = 1.1 s (MLS-series). The solid circles represent the results of laboratory experiments. The solid and dashed lines represent the numerical and analytical solutions, respectively. The results from laboratory experiments are in good agreement with those

from the analytical solution and numerical model. The amplitude of the MLS incident waves is chosen to provide the same steepness, $kH_0 = 0.076$, as the MSS waves. Hence, the wave patterns observed in the MSS-series (Fig.4) are similar to the results of the MLS-series.

Fig. 16 shows normalized wave heights along the vertical wall for the cases of MLM-series (H_0 = 0.054 m, T = 1.1 s). The incident wave amplitude is twice that of the cases of MSM-series, but the MLM-series have the same wave steepness kH_0 as MSM-series. For $\theta_0 = 10°$, the maximum value of the normalized wave height reached the uniform value of $H/H_0 \approx 1.65$, which shows an indication of the development of stem waves. Figs. 17 and 18 show normalized wave heights normal to the vertical wall at positions along $x = 6L$ and $15L$ for various incident angles. As shown in Figs. 17 and 18, stem waves appear for the cases of $\theta_0 = 10°$ and $20°$. The stem widths increase proportionally with the distance from the tip of the vertical wall. The width of the stem waves is found to decrease as the incident angle increases. The linear analytical solutions for small incident angles show large deviations from the measured results, which is consistent with previous results for the cases of MSM-series. On the other hand, the simulation results using the REF/DIF model are generally in good agreement with the results from laboratory experiments.

Figs. 19, 20, and 21 show comparisons of the measured, numerically simulated, and analytically calculated results of MLL-series (H_0 = 0.072 m, T = 1.1 s). In the results from the laboratory experiment, stem waves appear clearly at positions along $x = 6L$ and $15L$ for $\theta_0 = 10°$ and $20°$. The clear stem waves for periodic waves in the physical experiments are observed for the first time in this study. Berger and Kohlhase (1976) also conducted laboratory experiments to produce stem waves with a vertical wall. The experiments of Berger and Kohlhase (1976) were conducted in a constant water depth of $h = 0.25$ m for the wave length of L = 1.0 m with various incoming wave heights of $H_0 = 0.023 \sim 0.053$ m, and incidence angles of $\theta_0 = 10°,\ 15°, 20°,$ and $25°$. The experimental wave conditions of Berger and Kohlhase (1976) are similar to those of this study. The length of vertical wall (less than $9.8L$) used in the experiments of Berger and Kohlhase (1976), however, is much shorter than that of this study ($40L$ for the case of T = 0.7 s and $20L$ for the case of T = 1.1 s). Moreover, both ends of the vertical wall were open in the experiments of Berger and Kohlhase (1976), while a wave guide is installed from the wave generator to the tip of vertical wall in the present experiments, and the other end of the vertical wall is extended to the midst of 1/20 gravel beach. As a result, the wave heights along the wall measured by Berger and Kohlhase (1976) were contaminated by the parasitic waves diffracted by both ends of the wall. Thus, the stem waves developed along the wall were not clear in the results of Berger and Kohlhase (1976), while the stem waves observed in the present experiments are clearly noticeable.

Fig. 22(a) and 22(b) show the comparison of the three-dimensional plots of normalized wave height for MLS1 and MLL1 cases, respectively, based on the numerical results of REF/DIF. For the nonlinear case, the overall amplitudes are much smaller and the stem waves are developed along the wall as shown in Fig. 22(b). The stem wave height is nearly constant and the width of the stem waves tended to increase along the wall. Fig. 23(a) and Fig. 23(b) present the comparison of the three-dimensional plots of normalized free surface displacements for MLS1 and MLL1 cases, respectively. From Fig. 23(b) it can be seen that the stem waves propagate along the wall. Fig. 24 shows the contour plots of the instantaneous free surface

for MLS1 and MLL1 cases. The incident waves are reflected from the wall for the linear case. However, they are both refracted and partially reflected at the edge of stem region or the stem boundary as depicted also in Fig. 2.

In conclusion, the results of the laboratory experiments are in good agreement with those of the numerical simulations. However, the analytical solution cannot reproduce the stem waves. The widths of stem waves in the REF/DIF model are shown to be slightly broader than those of the results from laboratory experiments. This may be due to the fact that the REF/DIF model overestimates the nonlinearity of the waves. In addition, given the same incident angle condition, the stem waves in the cases of MLL-series show the largest stem width. Moreover, the widths of the stem waves tend to increase as the nonlinear property of the incident waves increases. This further demonstrates the effect of nonlinearity of incident waves on the development of stem waves as suggested by Yue and Mei (1980) and Yoon and Liu (1989).

4.3 Effects of nonlinearity

Yue and Mei (1980) proposed a single parameter, *K* given by Eq. (9), controlling the properties of stem waves developed along a vertical wedge based on the nonlinear Schrödinger equation. The *K* parameter represents both the nonlinearity of incident waves and the wedge slope. Yue and Mei (1980) proposed also a theoretical formula to estimate the amplitude squared of stem waves based on a simple shock model as:

$$|A_\infty/A_0|^2 = \frac{1}{2K}\left[2K + 1 + \sqrt{8K+1}\,\right] \tag{12}$$

where A_∞ is the amplitude of stem waves far from the tip of wedge along the vertical wall, A_0 is the amplitude of incident waves. In Fig. 25 the normalized wave height, H_∞/H_0, instead of A_∞/A_0, along the vertical wall is calculated using Eq. (1), and is compared with both the measured value and the theoretical one given by Eq. (12). A black solid line denotes the theoretical prediction by Yue and Mei (1980), red and blue solid lines represent the present numerical values for $\theta_0 = 10°$ and $20°$, respectively. The theoretical prediction of Yue and Mei (1980) overestimates slightly the stem heights in comparison with the measured values. The results from the present numerical simulation show a good agreement with the measured values. Moreover, the present numerical results show a dependence of stem heights on the angle of incidence. This implies that *K* is not a unique single parameter to control the property of stem waves.

The nonlinearity of monochromatic waves affects the wave property in two ways. Firstly, the wave length increases as the amplitude of waves increases. The nonlinear dispersion relationships can be obtained using the Stokes higher order theory. The nonlinear version of wave number, k_n, can be approximated by Eq. (5). Secondly, the wave shape becomes more peaked in its crest and broader in its trough due to the generation of higher harmonics. Regarding to stem waves it is well known that the nonlinear interaction between the incident and the reflected waves is responsible for the development of stem waves along the vertical wall. The overall consequence gained in the present study on the property of stem wave is that the

normalized stem height decreases and the stem width increases as the nonlinear parameter K increases, i.e., the incident height increases and the angle of incidence decreases. However, the details of the physical mechanism of nonlinear interaction are not clearly understood.

A simple and clear understanding of the role of wave nonlinearity on the development of stem waves is presented in this study. The crest lines of stem waves intersect a straight vertical wall normally, and, thus, the stem waves propagate along the wall with a uniform wave height. The region occupied by the stem waves increases with distance along the wall. In this study the role of the nonlinearity of waves affecting the stem property is investigated based on a simple geometrical relationship between the wave lengths of incident and stem waves. Fig. 26 shows a sketch for the definition of the properties of stem waves. In the figure, ϵ $(= \tan\theta_0)$ is the slope of vertical wall measured from the x-axis.

Yue and Mei (1980) proposed the slope ratio β of the edge line, i.e., stem boundary, of stem region denoted by dashed line in Fig. 26 as a function of K as:

$$\beta = \frac{1}{4}\left[3 + \sqrt{8K+1}\right] \tag{13}$$

Fig. 27 shows the comparison of the measured and numerically calculated β-values with that of Yue and Mei (1980). The β-values measured and calculated in this study are estimated based on the definition proposed by Berger and Kohlhase (1976). As shown in Fig. 27 the measured and calculated β-values agree well with each other, and show slightly different distributions depending on the angle of incidence. The β-values estimated using a simple shock theory of Yue and Mei (1980) deviate from the present results as K increases when $\theta_0 = 20°$. This slope ratio β of Yue and Mei (1980) can be converted to the angle of stem wedge α defined in Fig. 26(a) as:

$$\alpha = \tan^{-1}(\beta\epsilon) - \theta_0 \tag{14}$$

where $\beta\epsilon$ is the slope of the stem boundary as shown in Fig.26(a). On the other hand, this angle of stem wedge α can also be found simply by inspecting the geometrical relationship shown in Fig. 26(a). In the figure L_{n0} represents the wave length of incident waves, L_{ns} denotes the wave length of stem waves developed along the vertical wall, $y = -\epsilon x$. The wave lengths, L_{n0} and L_{ns}, are evaluated using the nonlinear wave number, k_n, given by Eq. (5). Thus, the amplitude of stem waves should be given to calculate L_{ns}. In this study the amplitude of stem waves is assumed to be known. The length, $L_{ns0}(= L_{n0}/\cos\theta_0)$, in the figure represents the wave length along the wall when no stem wave is assumed to be developed. When the stem waves are developed, the amplitude of stem waves is greater than that of incident waves. Thus, the wave length of stem waves, L_{ns}, is always greater than L_{ns0}. The geometrical relationship gives:

$$\tan\alpha = \frac{B}{L_{ns}} \quad \text{and} \quad B = \frac{L_{ns} - L_{ns0}}{\tan\theta_0} \tag{15}$$

Thus, the angle of stem wedge α can be found as:

$$\alpha = \tan^{-1}\left(\frac{L_{ns} - L_{ns0}}{L_{ns}\tan\theta_0}\right) \text{ or } \alpha = \tan^{-1}\left(\frac{L_{ns}\cos\theta_0 - L_{n0}}{L_{ns}\ \sin\theta_0}\right) \tag{16}$$

Another way to derive the stem angle α is presented based on wave ray theory as shown in Fig. 26(b). The wave rays of incident waves are refracted suddenly along the stem boundary (see Fig. 24) because the wave length of stem waves is longer than that of incident waves due to wave nonlinearity. As a result, the wave rays of stem waves are parallel to the vertical wall. The geometrical relationship between the rays and the wall gives:

$$L_{ns} = l\cos\alpha \text{ and } L_{n0} = l\sin\left(\frac{\pi}{2} - \theta_0 - \alpha\right) \tag{17}$$

One can easily get Eq. (16) by eliminating l from Eq. (17). Note that the incident waves are reflected not from the vertical wall, but from the stem boundary, and, thus, the incident waves are not perfectly reflected, but partially reflected.

If the amplitude of incident wave is small, the nonlinear wave number k_n becomes k, thus, $L_{ns} = L_{ns0}$, and $\alpha = 0$. As the amplitude of incident wave increases, the wave length of stem waves L_{ns} increases much more than L_{ns0} due to nonlinearity of waves. As a result, the angle of stem wedge α increases with increasing nonlinearity of incident waves and decreasing angle of incidence. Fig. 28 shows the comparison of the α-values evaluated using Eq. (14) of Yue and Mei (1980) and those using the empirical formula Eq. (16) proposed in this study along with the measured data. In the present empirical formula the amplitude of the stem waves is obtained from the numerical simulations to estimate the wave length of stem waves, while the measured angle of stem wedge is directly obtained from the experimental data using the definition of stem region proposed by Berger and Kohlhase (1976). Good agreement is observed between the measured and theoretical α-values. The present empirical formula gives slightly larger α-values than Yue and Mei (1980) for larger angle of incidence. This geometrical analysis supports strongly that the increase of wave length due to wave nonlinearity is responsible for the development of stem waves along a vertical wall.

5 Conclusions

In this study, precisely controlled experiments are conducted to investigate the existence and the properties of stem waves developed along a vertical wedge for the cases of monochromatic waves. Numerical and analytical solutions are also obtained and compared with the measured data. The key results derived from this study are here illustrated:

1. For small amplitude waves, the wave height along the wall shows a slowly varying undulation with the average value of H/H_0=2.0. The maximum value of undulation is approximately $H/H_0 \approx$2.3, and the distance from the tip to the location of maximum wave height decreases with increasing angle of incidence. Normalized wave heights perpendicular to the wall show a standing wave pattern. In particular, the wave height distribution does not support the generation of stem waves. Both numerical and linear analytical solutions agree well with measured wave heights.

2. As the amplitude of incident waves increases, both the undulation intensity and the asymptotic normalized wave height decrease along the wall. For larger amplitude waves with smaller angle of incidence, i.e., larger *K* values, the measured data show clear stem waves along the wall. Numerical simulation results are in good agreement with the results of laboratory experiments, while the linear analytical solution gives no stem wave.

3. Stem waves can be developed when the nonlinear parameter *K* is greater than 0.43. As the nonlinear parameter K increases, the stem waves become stronger, i.e., the normalized stem height decreases and the stem width increases.

4. It is found from a simple geometric investigation that the lengthening of wave length due to the nonlinearity of waves is responsible for the development of stem waves along the wall. As a result, the incident waves are suddenly refracted along the stem boundary to form stem waves, and are also partially reflected from the stem boundary. These are consistent with the facts reported earlier by previous researchers.

5. The existence and the properties of stem waves for sinusoidal waves found theoretically via numerical simulations are fully supported by the physical experiments conducted in this study. Experimental data obtained in this study can be used as a useful tool to verify nonlinear dispersive wave numerical models.

Acknowledgment

This study was performed by a project of “Investigation of large swell waves and rip currents and development of the disaster response system (No. 20140057)” sponsored by the Ministry of Oceans and Fisheries of Korea.

References

Berger, U. and Kohlhase, S.: Mach-reflection as a diffraction problem, Proc. 15th Conf. Coastal Engng. , 796-814, 1976.

Chen, H. S.: Combined reflection and diffraction by a vertical wedge, Tech. Rep. CERC 87-16, U.S. Army Corps of Engrs. (USACE) Wtrwy. Experiment Station, Vicksburg, Miss., USA, 1987.

Kadomtsev, B. and Petviashvili, V.: On the stability of solitary waves in weakly dispersing media, Sov. Phys. Dokl, 539-541, 1970.

Kirby, J. T. and Dalrymple, R. A.: Combined refraction/diffraction model REF/DIF 1, Version 3.0: Documentation and User's Manual, Center for Applied Coastal Research, Department of Civil Engineering, University of Delaware, Delaware, USA, 2002.

Le Mehaute, B.: An introduction to hydrodynamics and water waves, Springer, 1976.

Lee, J.-I., Kim, Y.-T., and Cho. Y.-S.: Hydraulic model test for stem waves along vertical wall under regular wave actions, Proc. of Annual Conf. of Korean Society of Civil Engineers, 4939-4943, 2003 (in Korean).

Lee, J. I. and Yoon, S. B.: Hydraulic and numerical experiments of stem waves along a vertical wall, Journal of the Korean Society of Civil Engineers, 26, 405-412, 2006 (in Korean).

Lee, J. and Kim, Y.: Numerical analysis of stem waves along a vertical wall, Journal of Coastal Research, 1101-1105, 2007.

Liu, P. L. F. and Yoon, S. B.: Stem waves along a depth discontinuity, Journal of Geophysical Research: Oceans, 91, 3979-3982, 1986.

Mase, H., Memita, T., Yuhi, M., and Kitano, T.: Stem waves along vertical wall due to random wave incidence, Coastal Engineering, 44, 339-350, 2002.

Melville, W.: On the mach reflexion of a solitary wave, J. of Fluid Mech., 98, 285-297, 1980.

Mei, C. C., Stiassnie, M., and Yue, D. K.-P.: Theory and applications of ocean surface waves: Part 1: Linear aspects Part 2: Nonlinear aspects, World Scientific, 1989.

Nicholls, D. P.: On hexagonal gravity water waves, Mathematics and computers in simulation, 55, 567-575, 2001.

Perroud, P. H.: The solitary wave reflection along a straight vertical wall at oblique incidence, IER Report. 99-3,93. University of California, Berkeley, Calif, USA, 1957.

Postacchini, M., Brocchini, M., and Soldini, L.: Vorticity generation due to cross-sea, J. of Fluid Mech., 744, 286-309, 2014.

Sommerfeld, A.: Mathematische theorie der diffraction, Mathematische Annalen, 47, 317-374, 1896.

Suh, K. D., Park, W. S., and Park, B. S.: Separation of incident and reflected waves in wave–current flumes, Coastal Engineering, 43, 149-159, 2001.

Yoon, S. B. and Liu, P. L.-F.: Stem waves along breakwater, Journal of waterway, port, coastal, and ocean engineering, 115, 635-648, 1989.

Yue, D. K. and Mei, C. C.: Forward diffraction of Stokes waves by a thin wedge, J. of Fluid Mech., 99, 33-52, 1980.

Table 1 Experimental wave conditions.

Test case	Water depth h (m)	Wave period T (s)	Wave height H_0 (m)	Incident angle θ_0 (deg.)	Nonlinearity	
					Wave steepness kH_0	Nonlinear parameter K
MSS1	0.25	0.7	0.009	10	0.076	0.088
MSS2				20		0.021
MSS3				30		0.008
MSS4				40		0.004
MSM1			0.027	10	0.229	0.793
MSM2				20		0.186
MSM3				30		0.074
MSM4				40		0.035
MSL1			0.036	10	0.305	1.411
MSL2				20		0.331
MSL3				30		0.132
MSL4				40		0.062
MLS1		1.1	0.018	10	0.076	0.123
MLS2				20		0.029
MLS3				30		0.011
MLS4				40		0.005
MLM1			0.054	10	0.228	1.108
MLM2				20		0.260
MLM3				30		0.103
MLM4				40		0.049
MLL1			0.072	10	0.304	1.969
MLL2				20		0.462
MLL3				30		0.184
MLL4				40		0.087

Table 2 Measuring points in hydraulic experiments.

Wave period (T)	x-dir. (along the wall)	y-dir. (normal to the wall)	
		at x/L = 6	at x/L = 15
0.7 sec	x = 0.0 m~11.4 m (Δx = 0.2 m)	y = 0.1 m~3.7 m (Δy = 0.1 m)	
1.1 sec	x = 0.0 m~22.8 m (Δx = 0.4 m)	y = 0.2 m~7.3 m (Δy = 0.2 m)	

Photo 1. Experimental facility and wave gauge array.

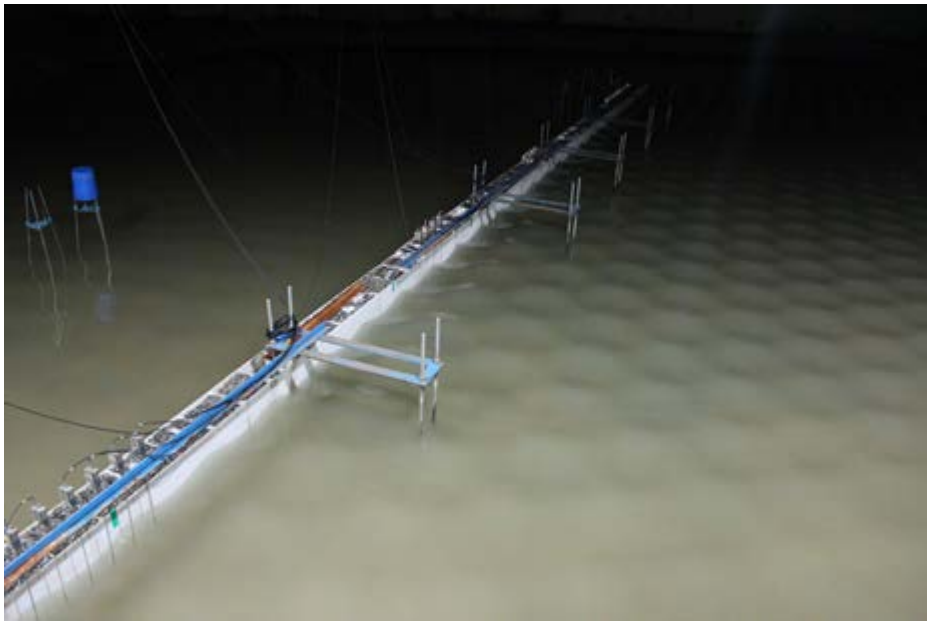

Photo 2. Wave pattern in front of a vertical wall ($\theta_0 = 30°$).

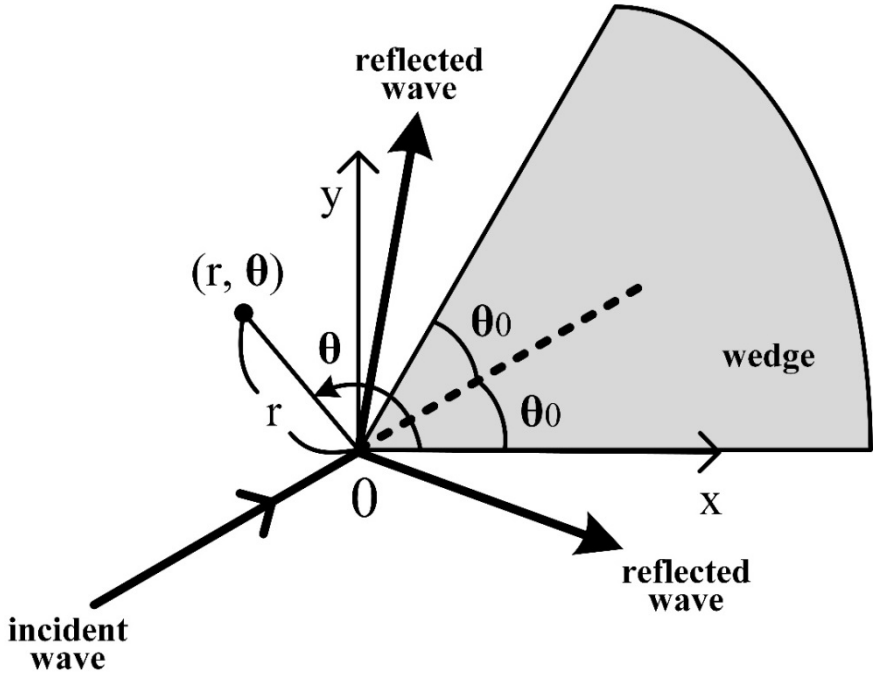

Figure 1. Definition sketch of wave field around a vertical wedge.

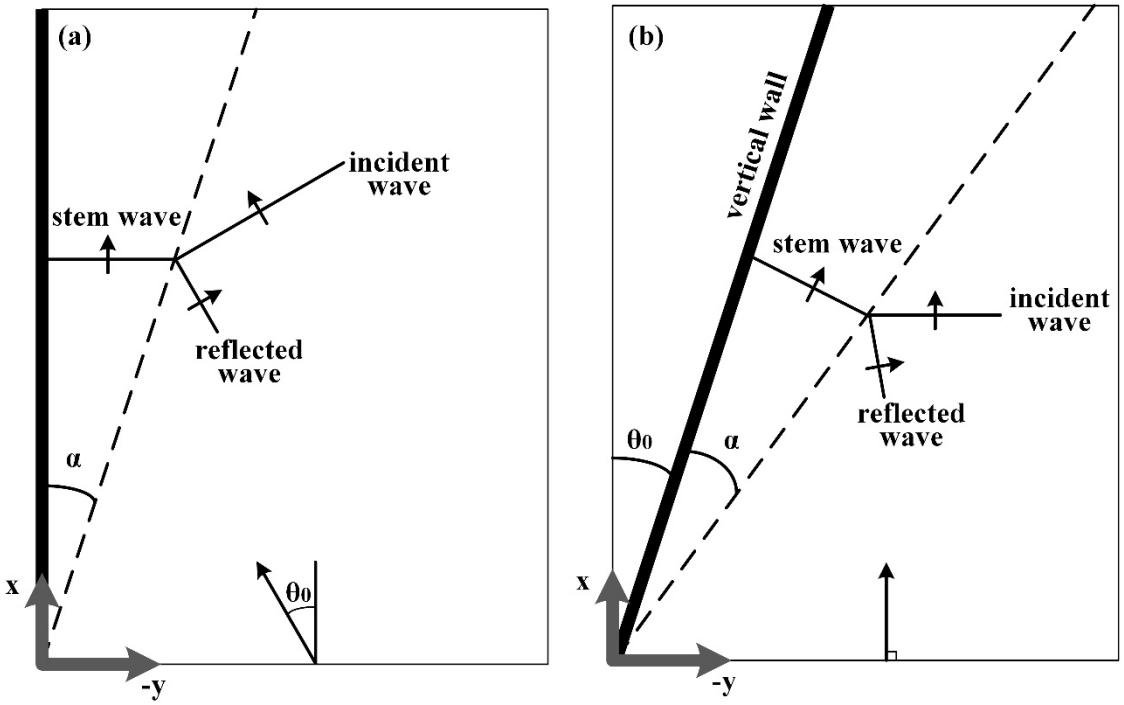

Figure 2. Coordinate system for numerical simulations: (a) present, (b) Yue & Mei (1980).

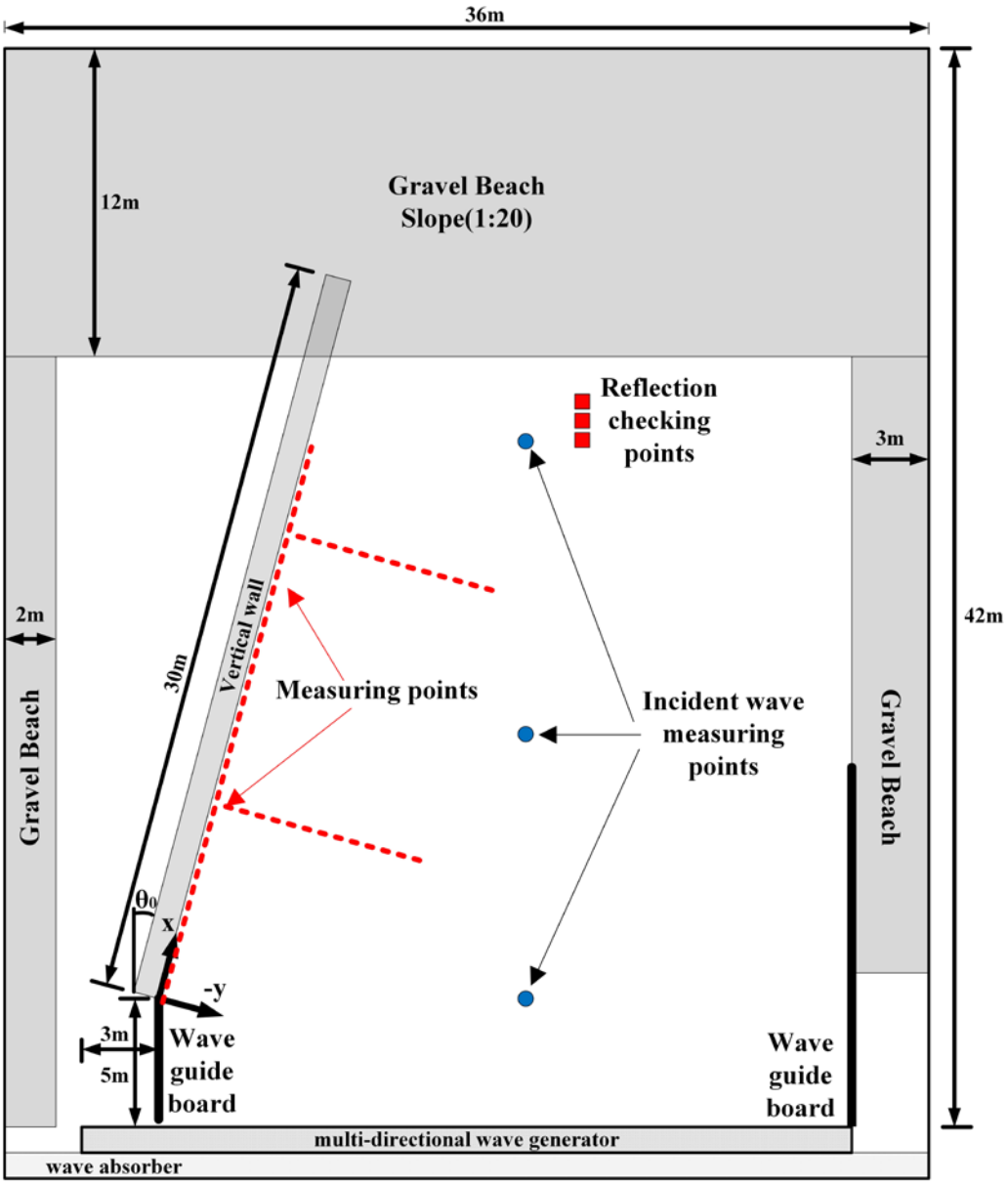

Figure 3. Definition sketch of experimental setup.

5

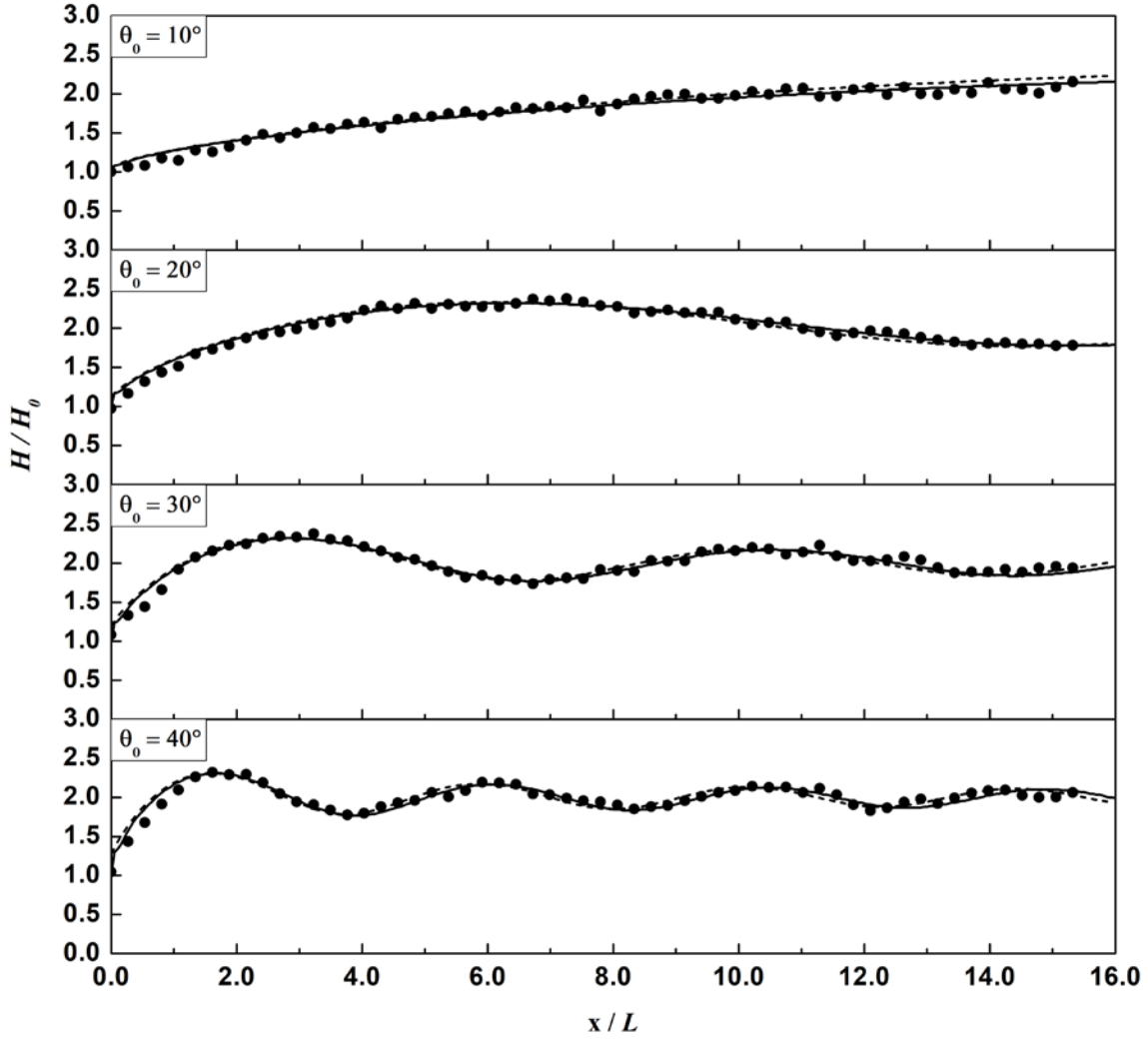

Figure 4. Normalized wave heights along the wall for the cases of MSS1 ~ MSS4. Solid circle: measured, solid line: present numerical, dashed line: analytical (Chen, 1987).

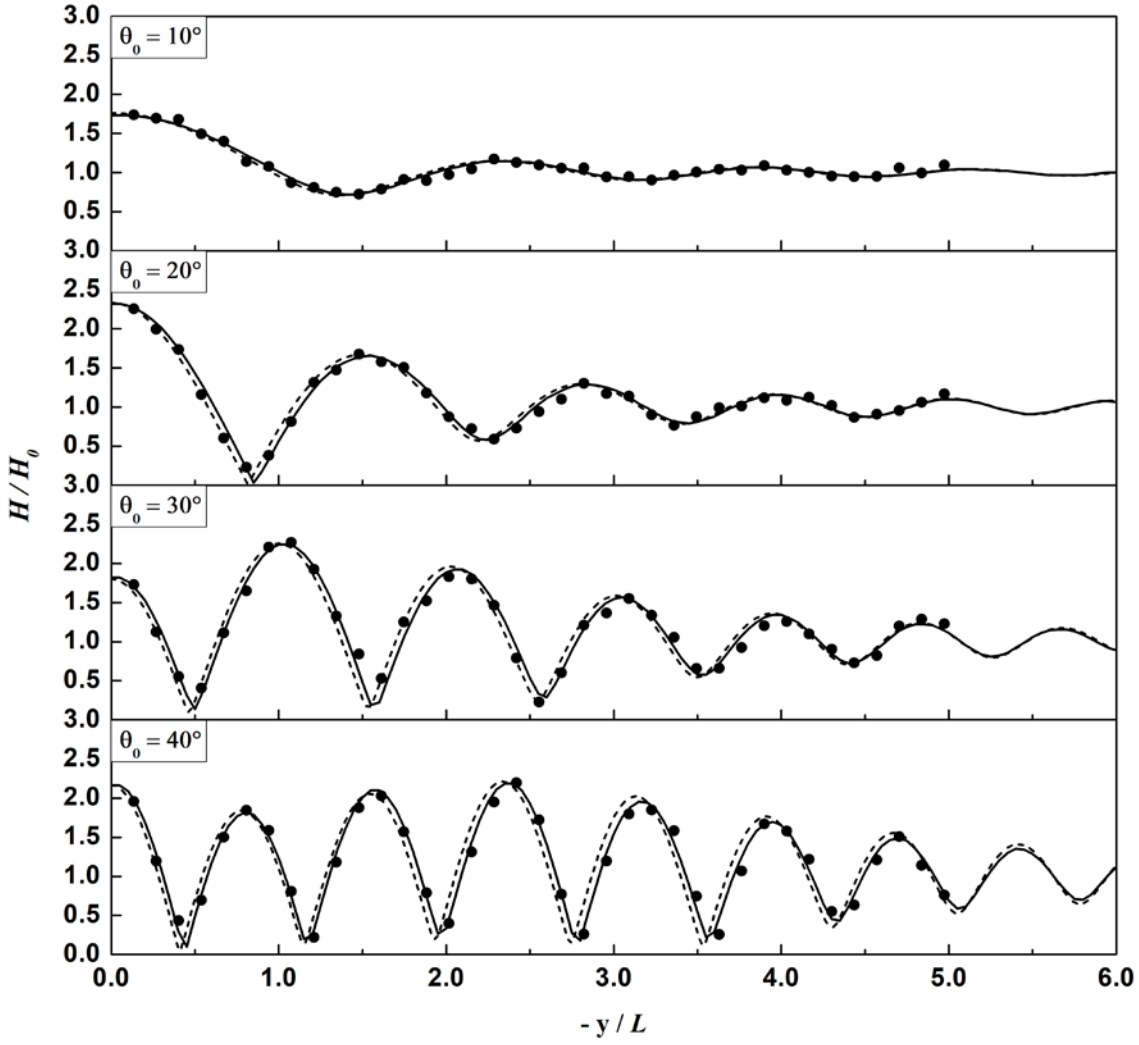

Figure 5. Normalized wave heights normal to the wall at $x = 6L$ for the cases of MSS1 ~ MSS4. Solid circle: measured, solid line: present numerical, dashed line: analytical (Chen, 1987).

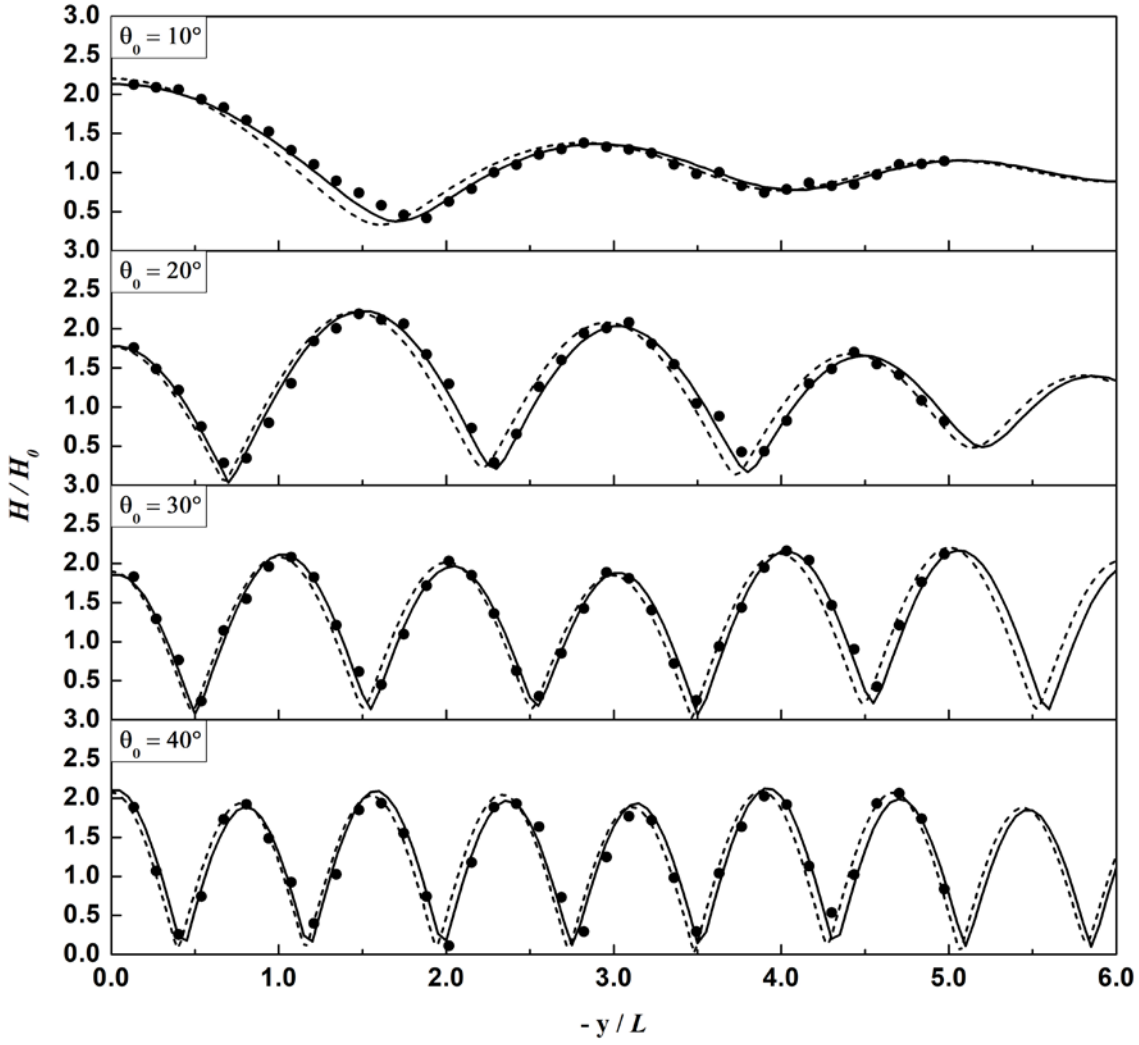

Figure 6. Normalized wave heights normal to the wall at $x = 15L$ for the cases of MSS1 ~ MSS4. Solid circle: measured, solid line: present numerical, dashed line: analytical (Chen, 1987).

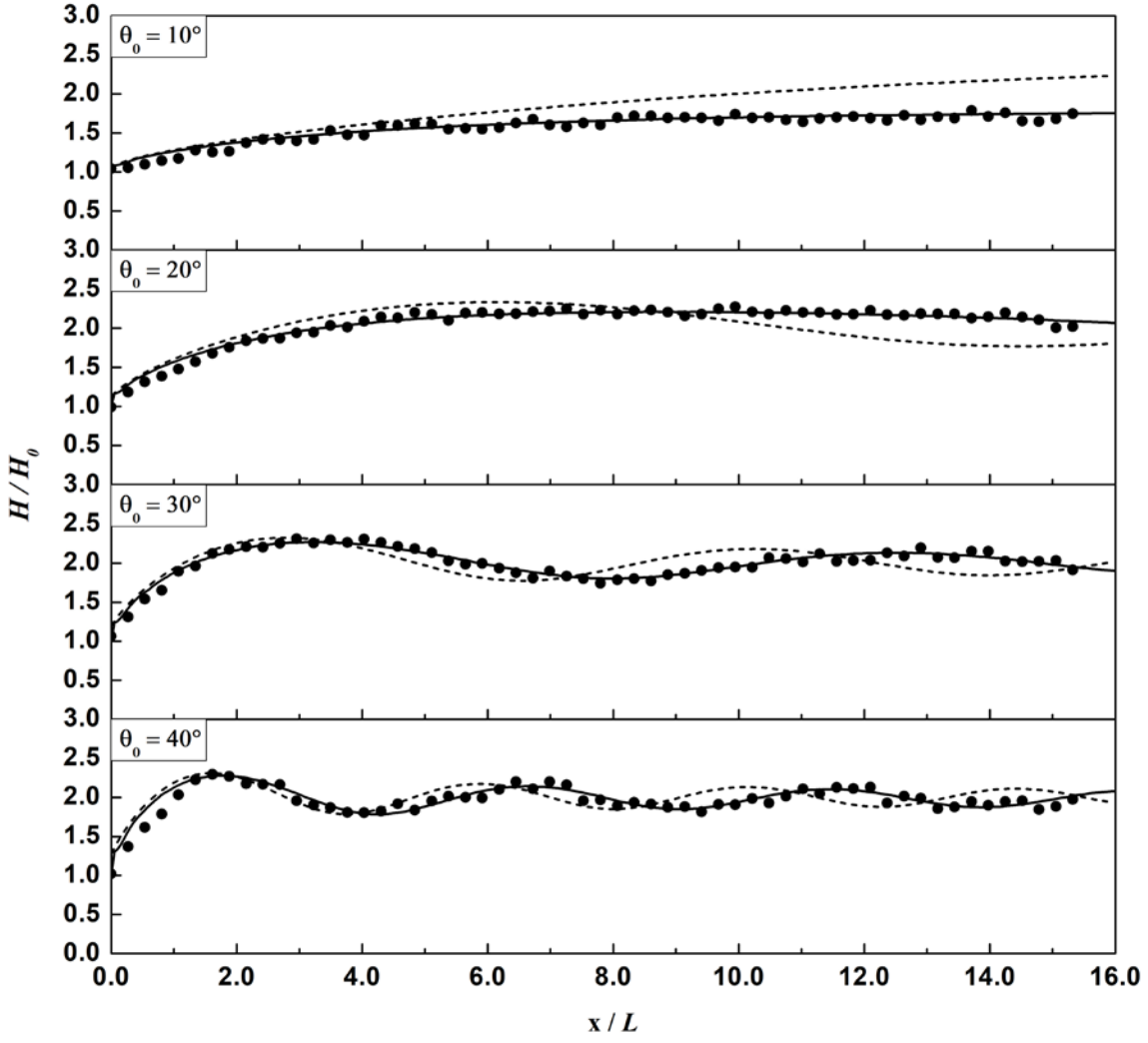

Figure 7. Normalized wave heights along the wall for the cases of MSM1 ~ MSM4. Solid circle: measured, solid line: present numerical, dashed line: analytical (Chen, 1987).

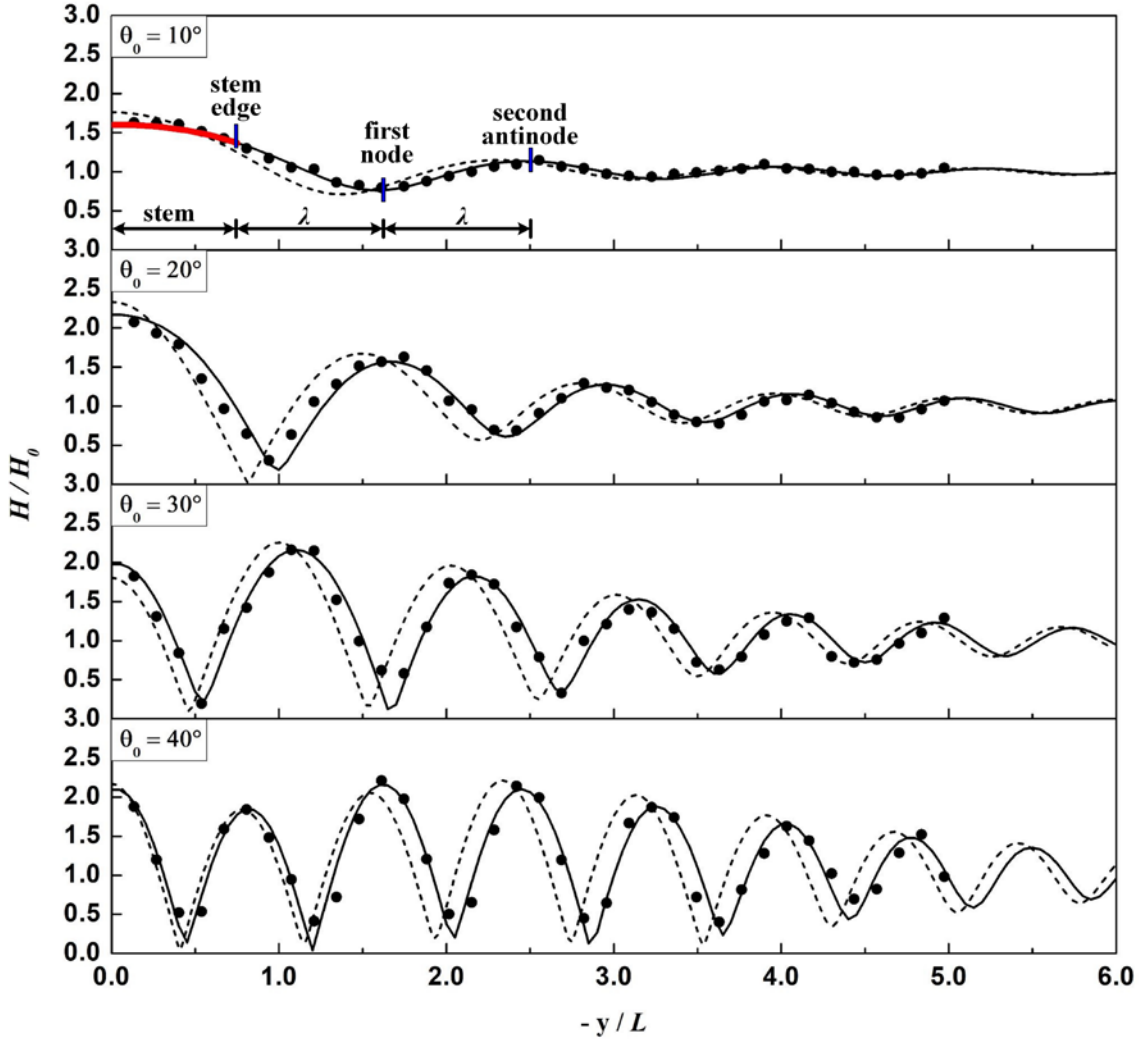

Figure 8. Normalized wave heights normal to the wall at $x = 6L$ for the cases of MSM1 ~ MSM4. Solid circle: measured, solid line: present numerical, dashed line: analytical (Chen, 1987).

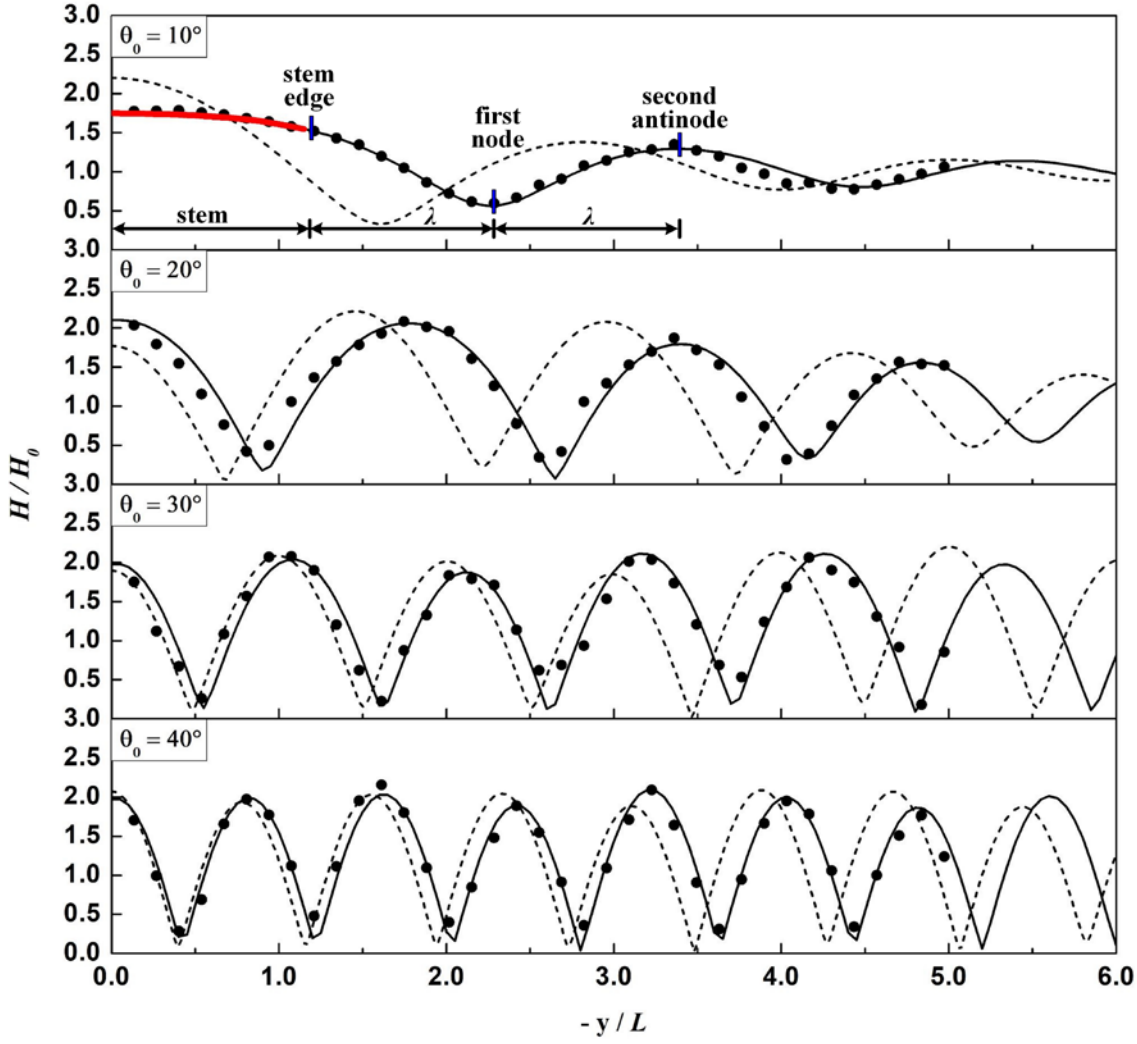

Figure 9. Normalized wave heights normal to the wall at $x = 15L$ for the cases of MSM1 ~ MSM4. Solid circle: measured, solid line: present numerical, dashed line: analytical (Chen, 1987).

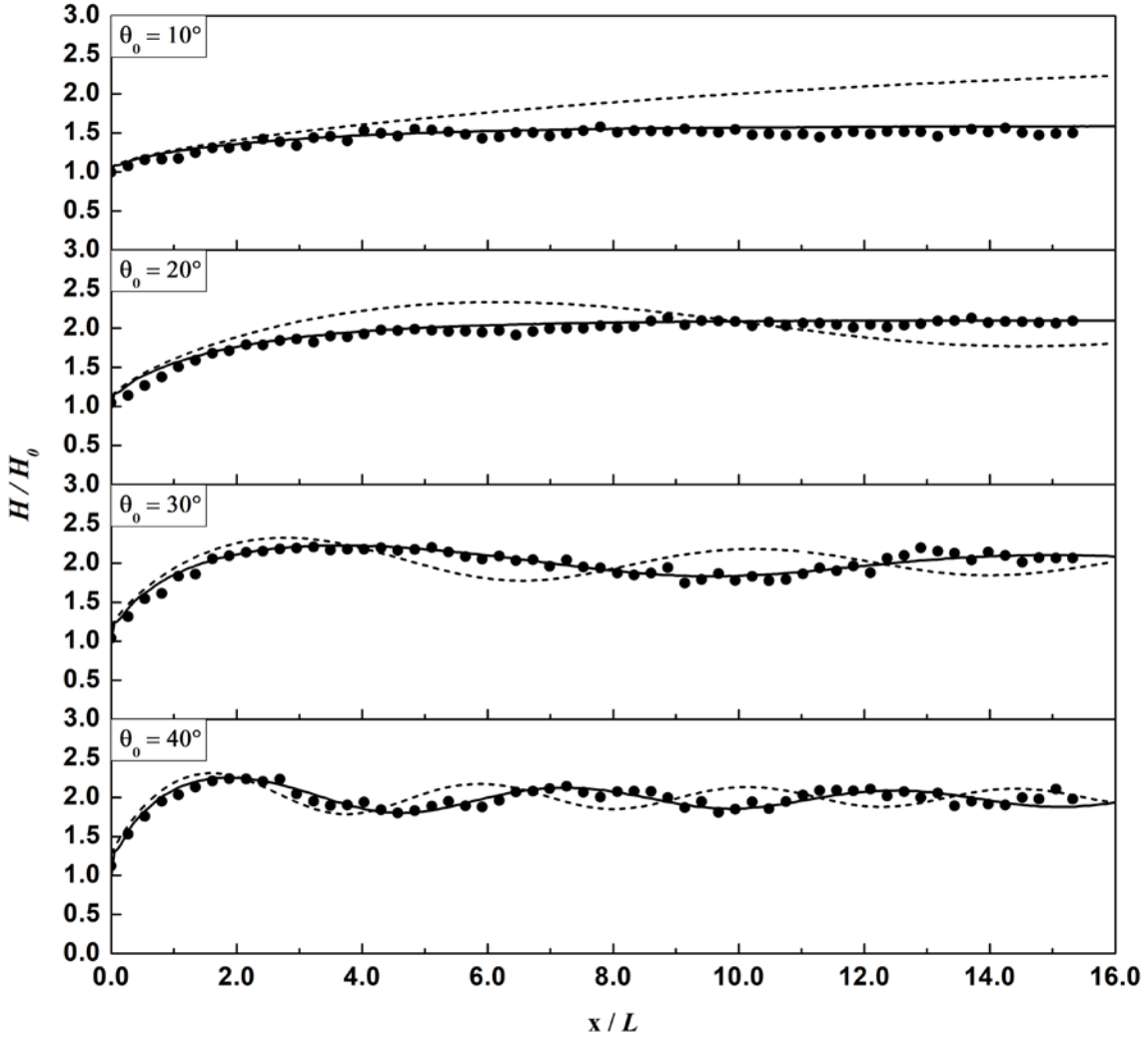

Figure 10. Normalized wave heights along the wall for the cases of MSL1 ~ MSL4. Solid circle: measured, solid line: present numerical, dashed line: analytical (Chen, 1987).

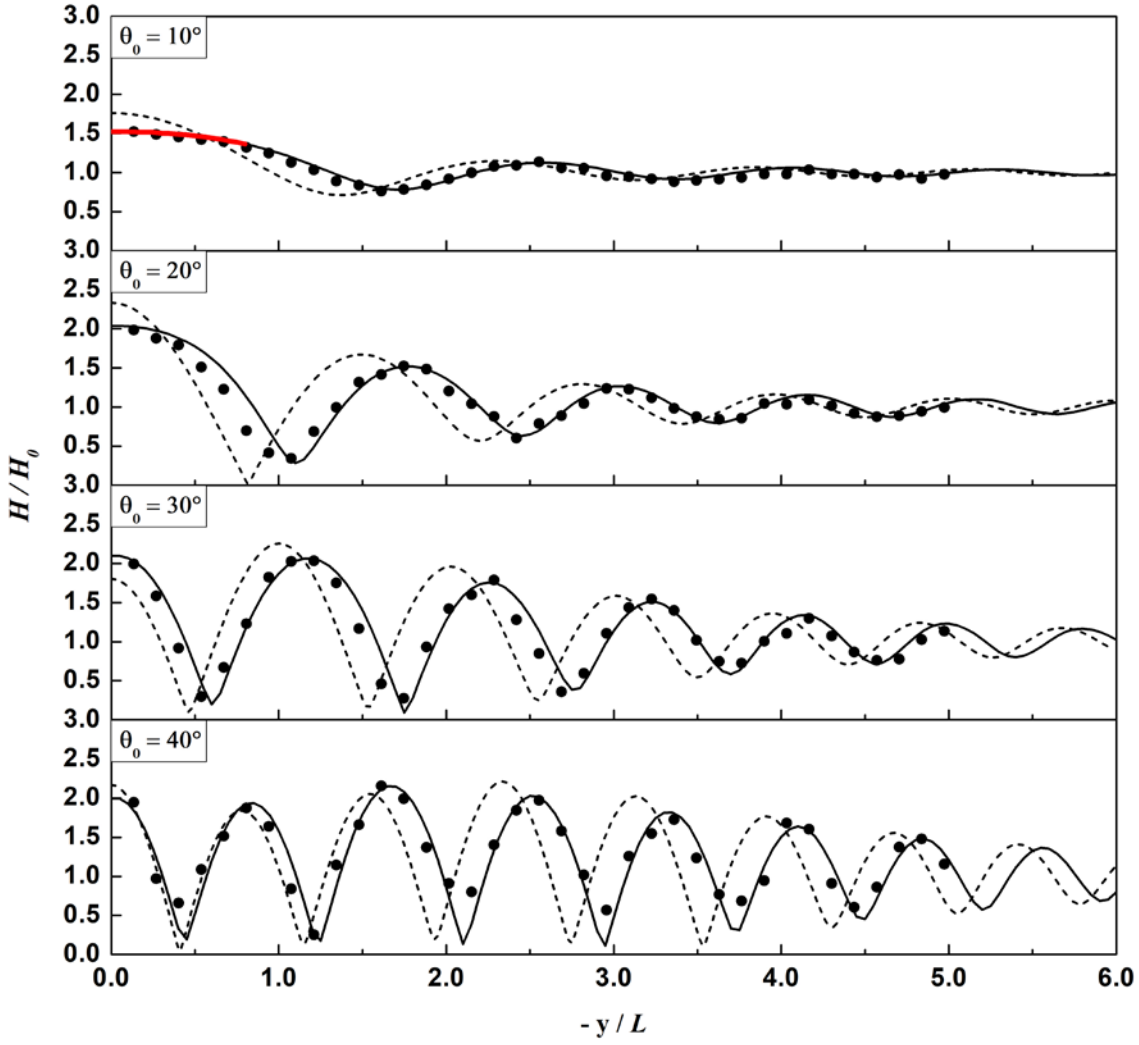

Figure 11. Normalized wave heights normal to the wall at $x = 6L$ for the cases of MSL1 ~ MSL4. Solid circle: measured, solid line: present numerical, dashed line: analytical (Chen, 1987).

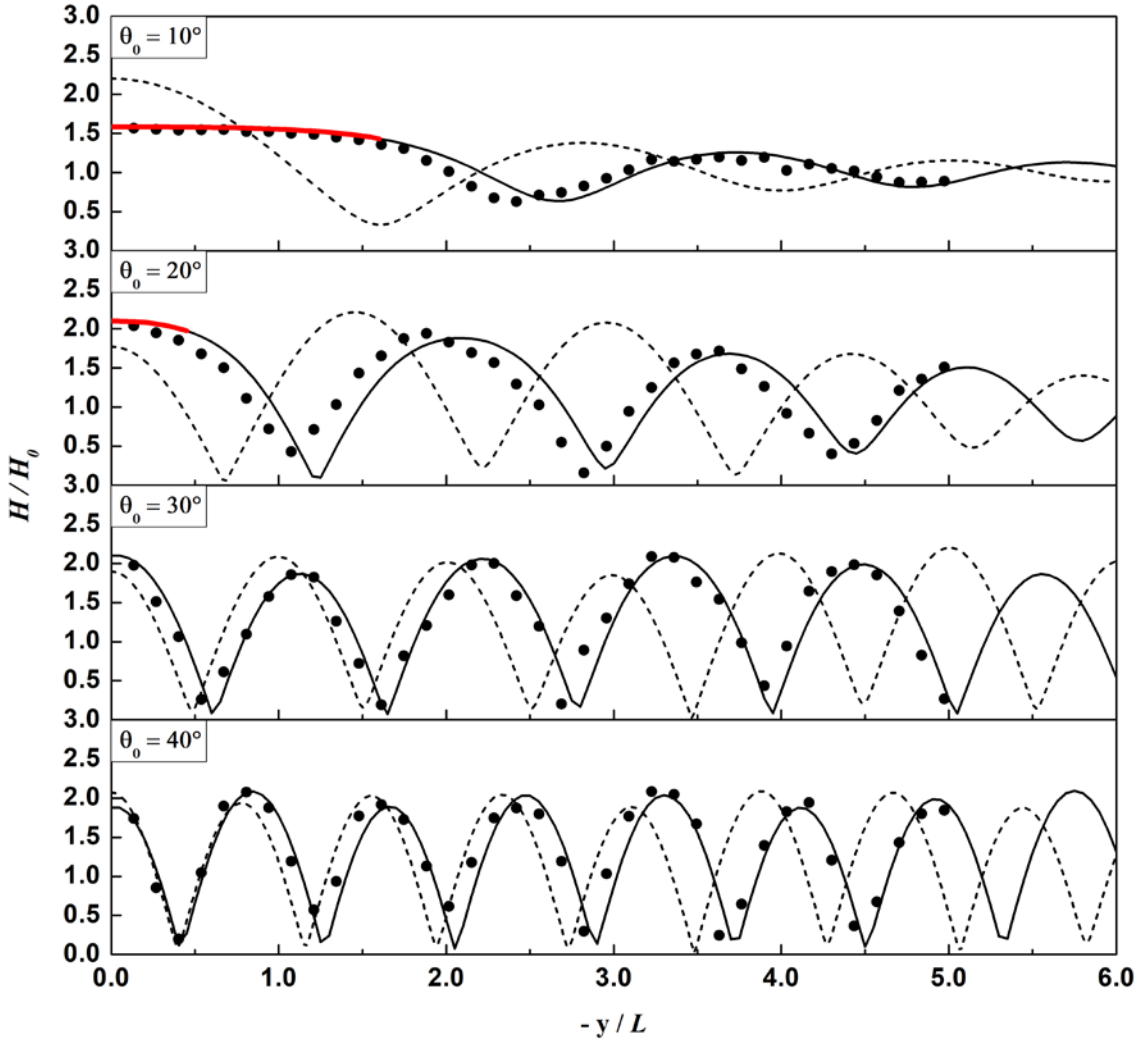

Figure 12. Normalized wave heights normal to the wall at $x = 15L$ for the cases of MSL1 ~ MSL4. Solid circle: measured, solid line: present numerical, dashed line: analytical (Chen, 1987).

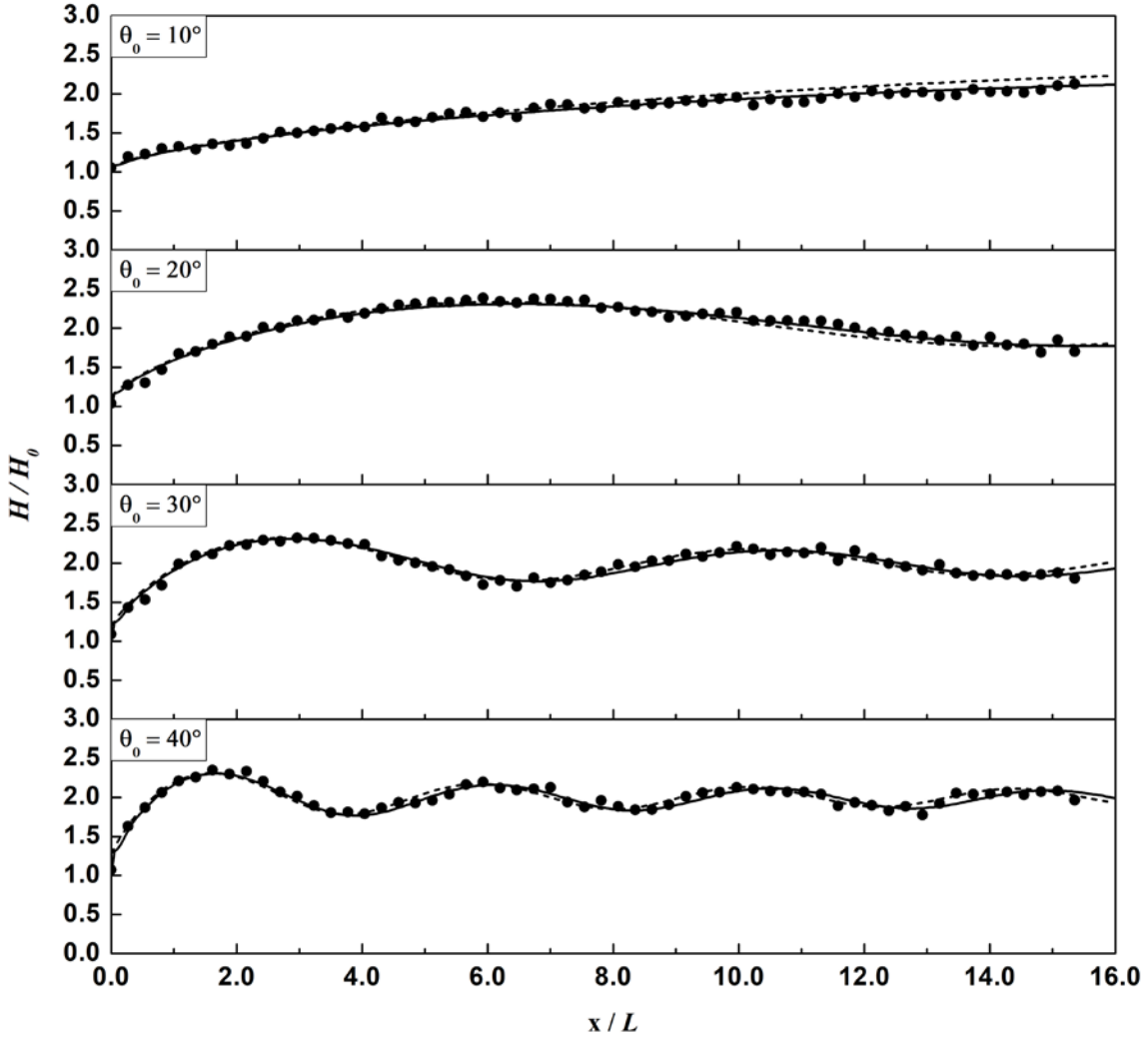

Figure 13. Normalized wave heights along the wall for the cases of MLS1 ~ MLS4. Solid circle: measured, solid line: present numerical, dashed line: analytical (Chen, 1987).

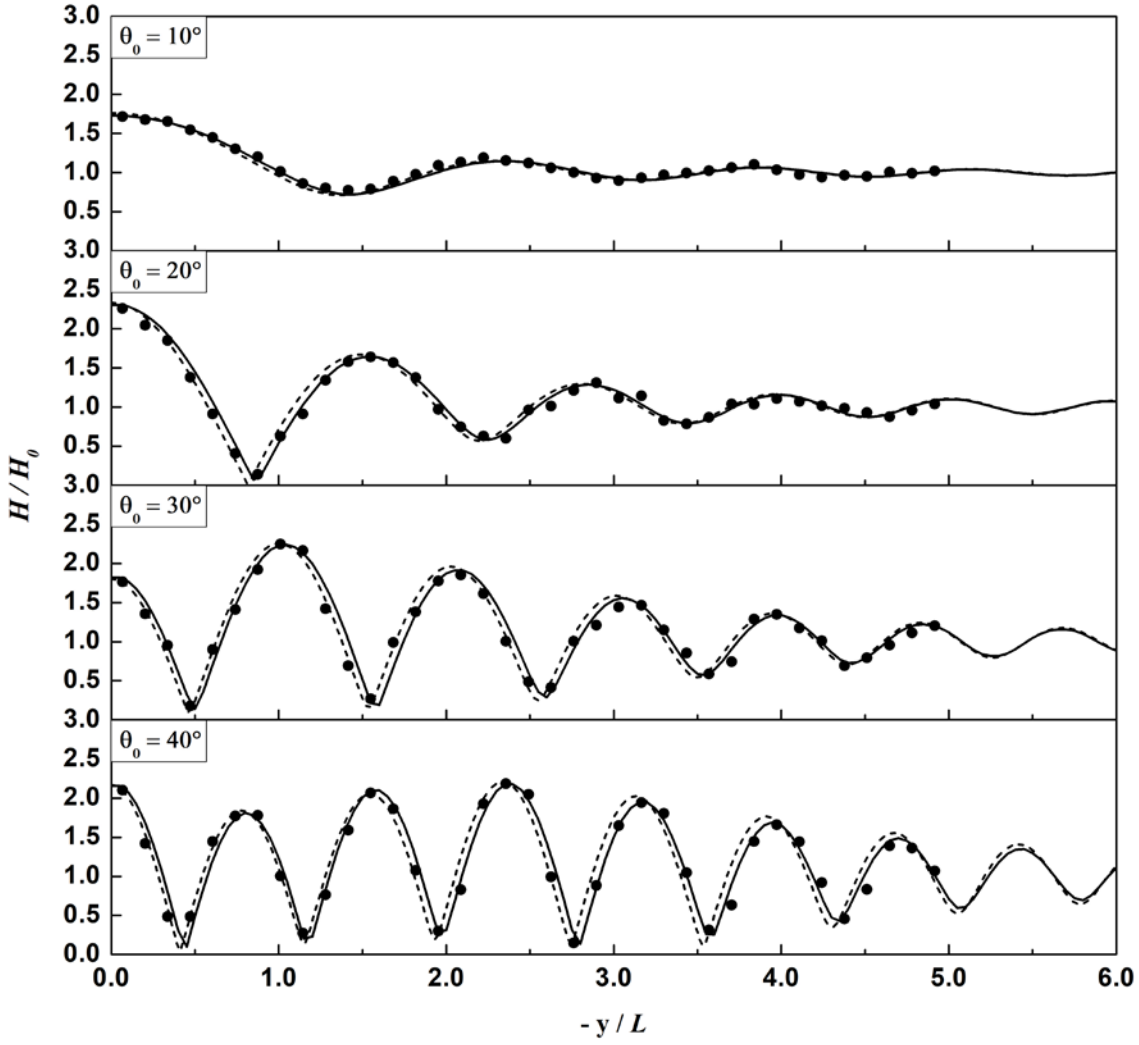

Figure 14. Normalized wave heights normal to the wall at $x = 6L$ for the cases of MLS1 ~ MLS4. Solid circle: measured, solid line: present numerical, dashed line: analytical (Chen, 1987).

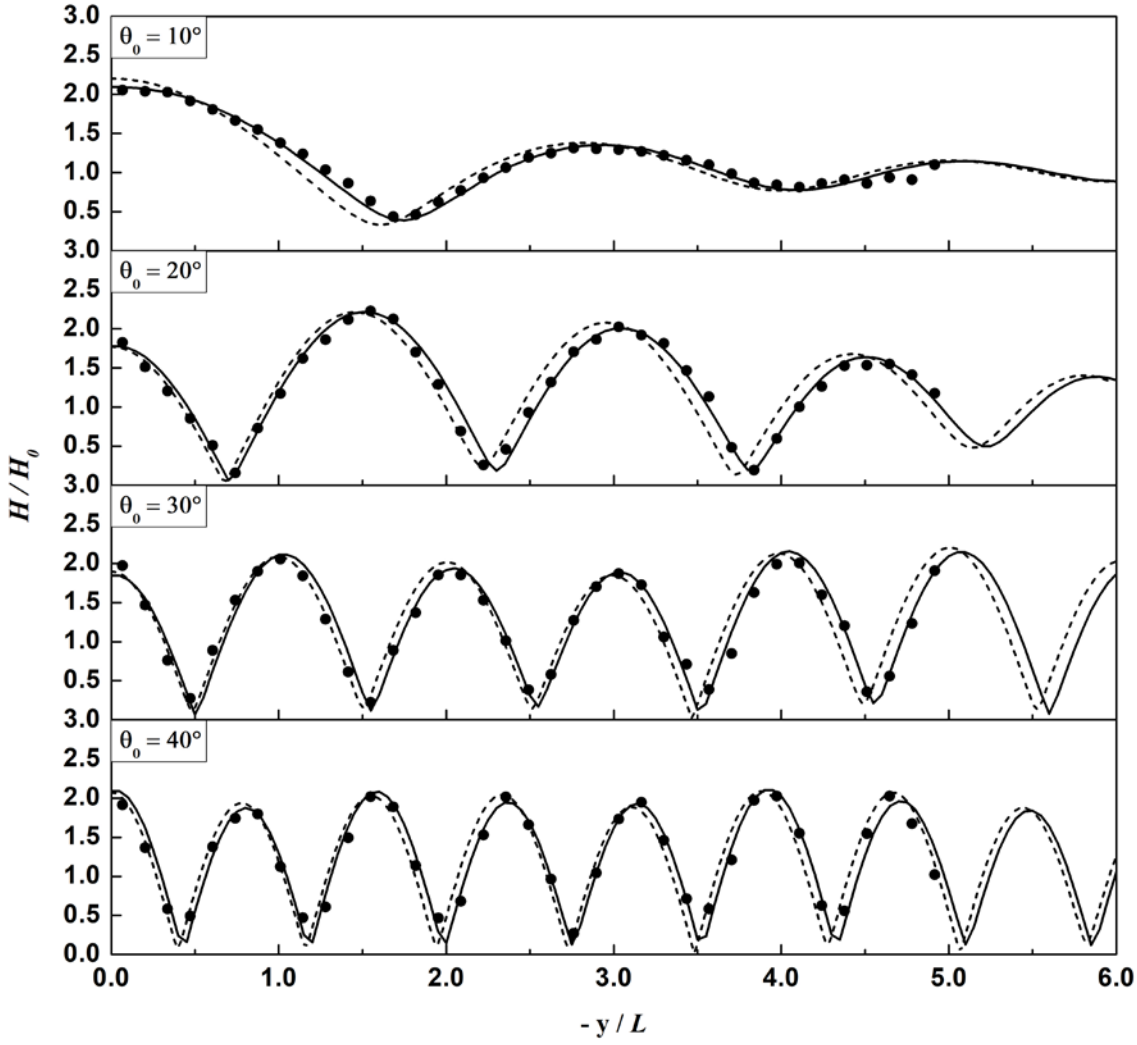

Figure 15. Normalized wave heights normal to the wall at $x = 15L$ for the cases of MLS1 ~ MLS4. Solid circle: measured, solid line: present numerical, dashed line: analytical (Chen, 1987).

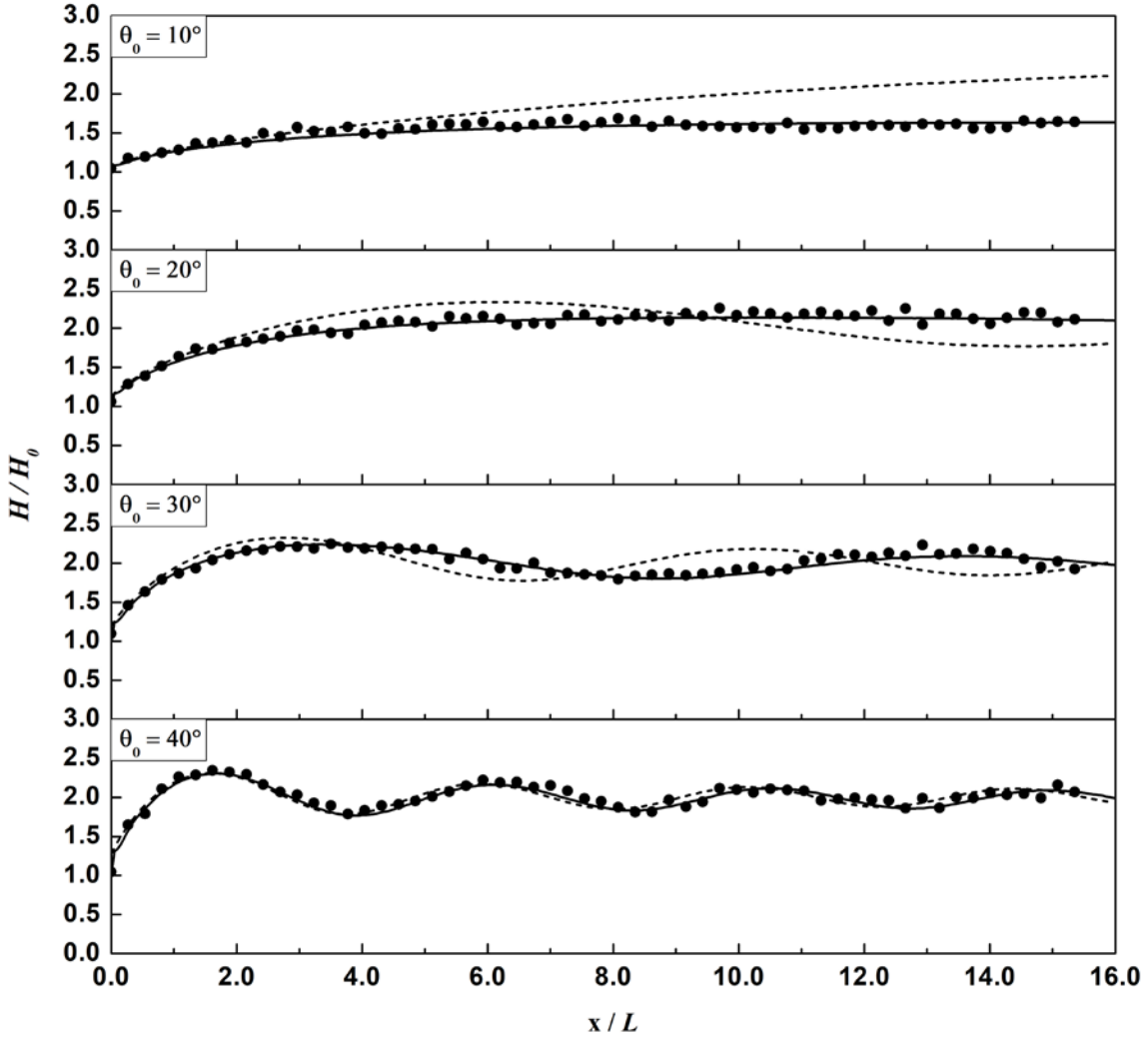

Figure 16. Normalized wave heights along the wall for the cases of MLM1 ~ MLM4. Solid circle: measured, solid line: present numerical, dashed line: analytical (Chen, 1987).

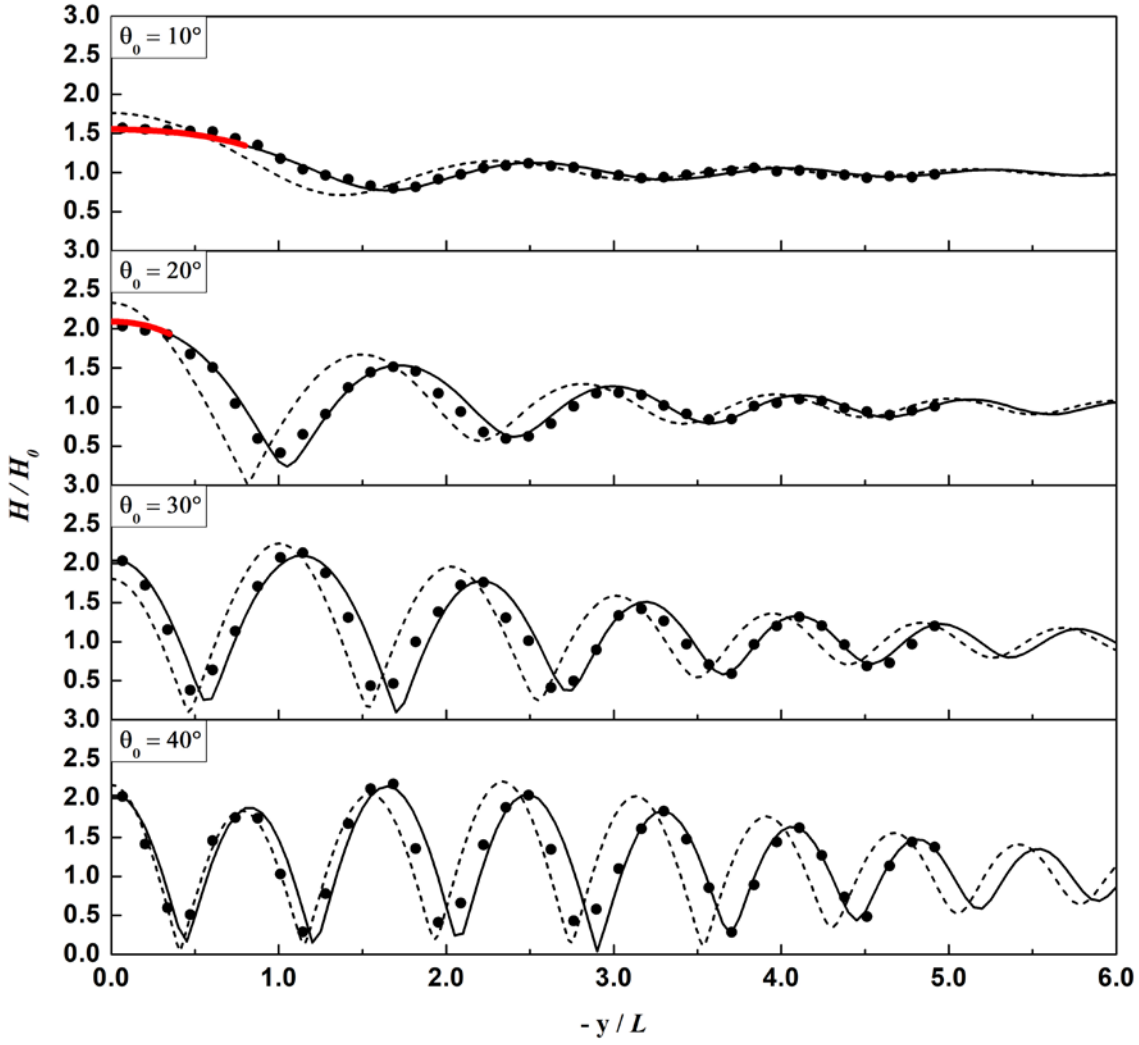

Figure 17. Normalized wave heights normal to the wall at $x = 6L$ for the cases of MLM1 ~ MLM4. Solid circle: measured, solid line: present numerical, dashed line: analytical (Chen, 1987).

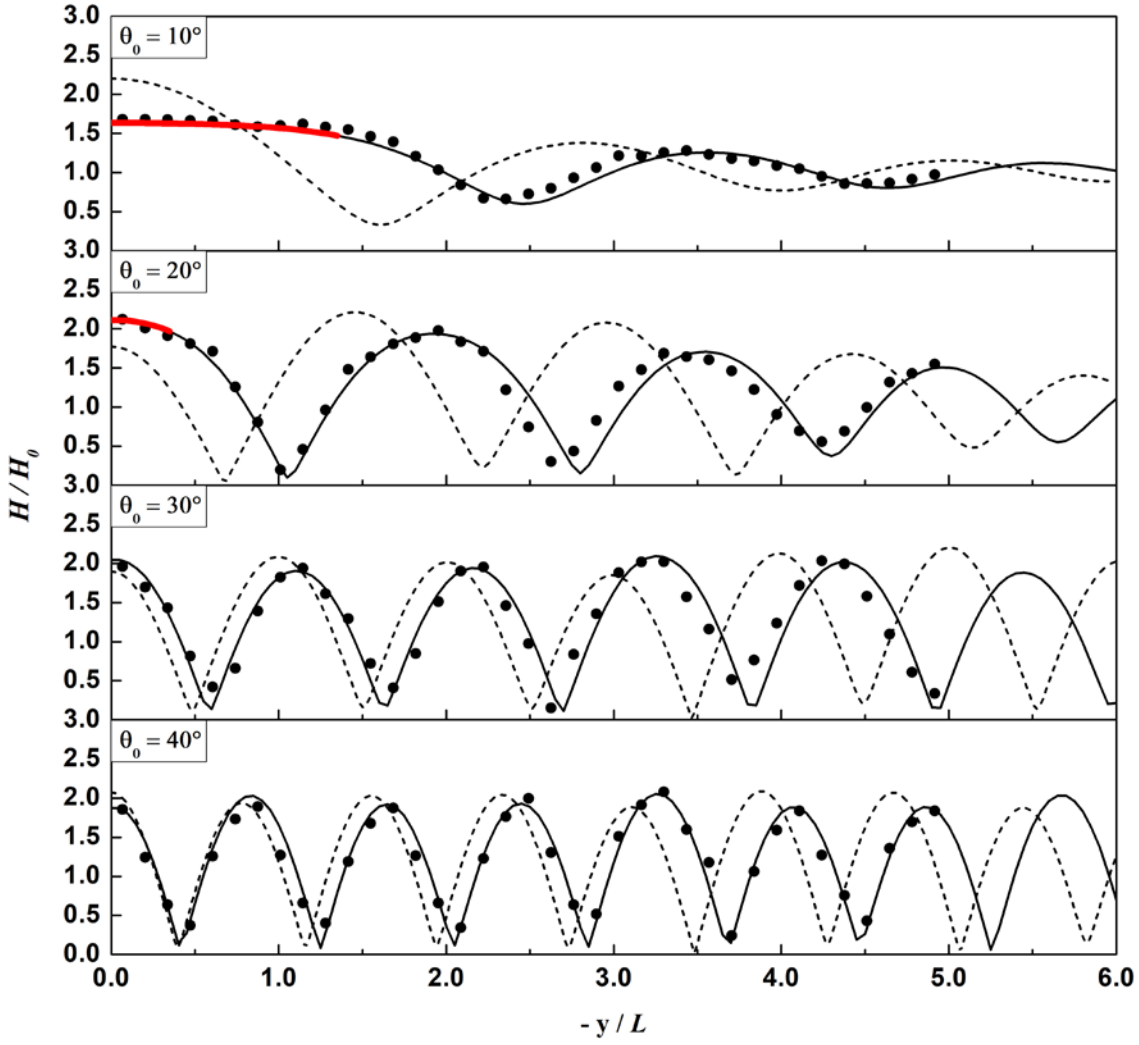

Figure 18. Normalized wave heights normal to the wall at $x = 15L$ for the cases of MLM1 ~ MLM4. Solid circle: measured, solid line: present numerical, dashed line: analytical (Chen, 1987).

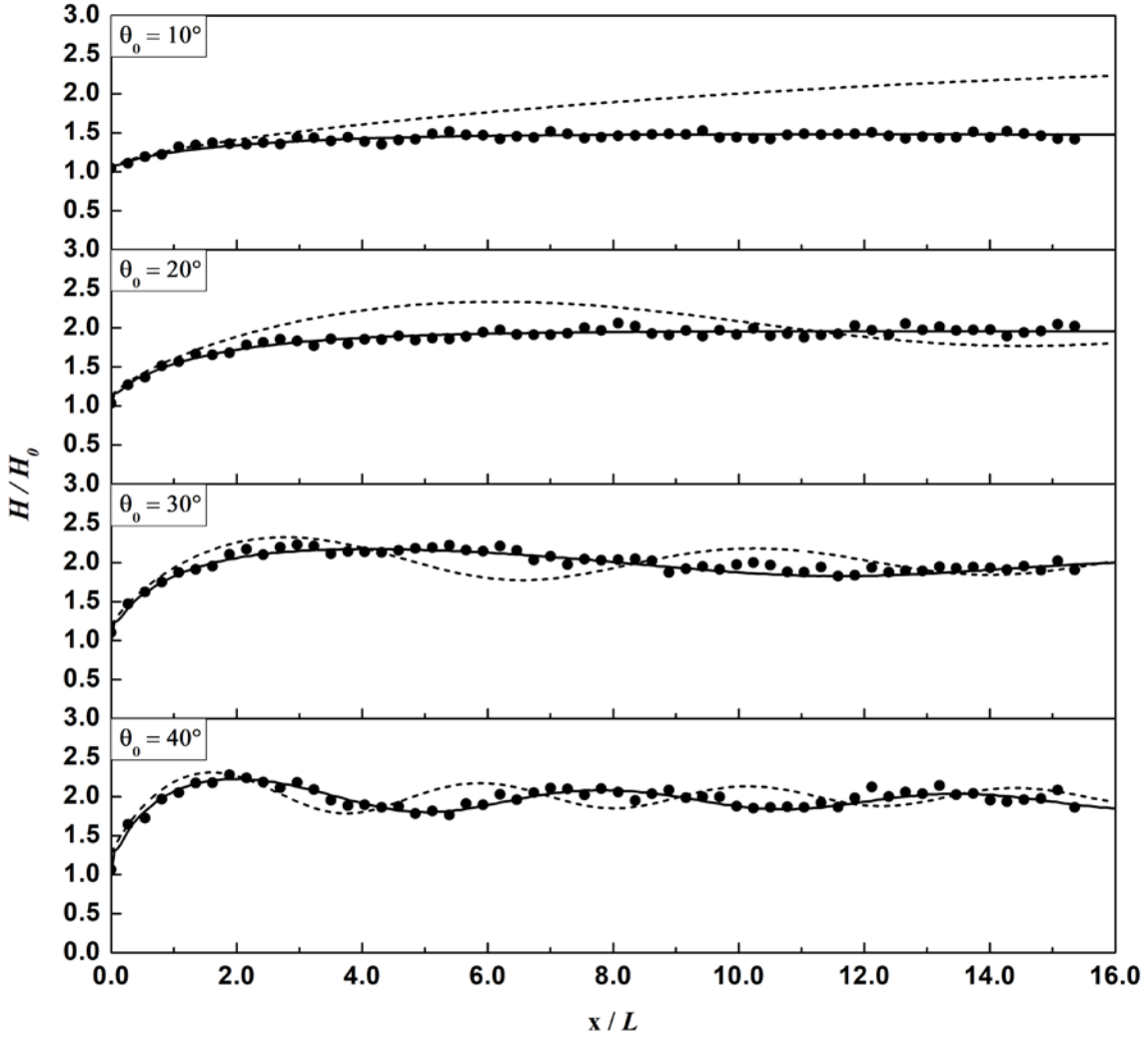

Figure 19. Normalized wave heights along the wall for the cases of MLL1 ~ MLL4. Solid circle: measured, solid line: present numerical, dashed line: analytical (Chen, 1987).

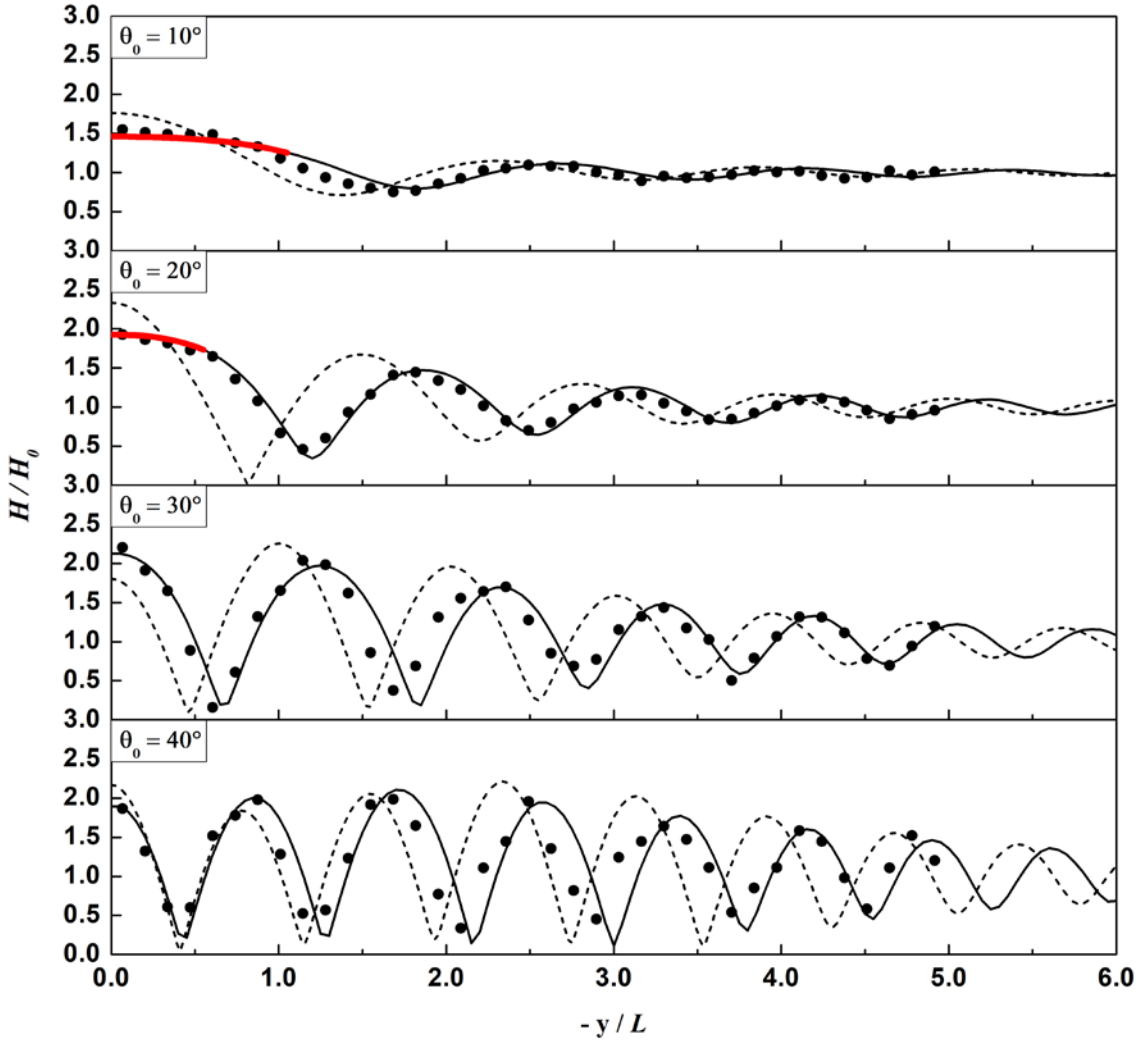

Figure 20. Normalized wave heights normal to the wall at $x = 6L$ for the cases of MLL1 ~ MLL4. Solid symbol: measured, solid line: present numerical, dashed line: analytical (Chen, 1987).

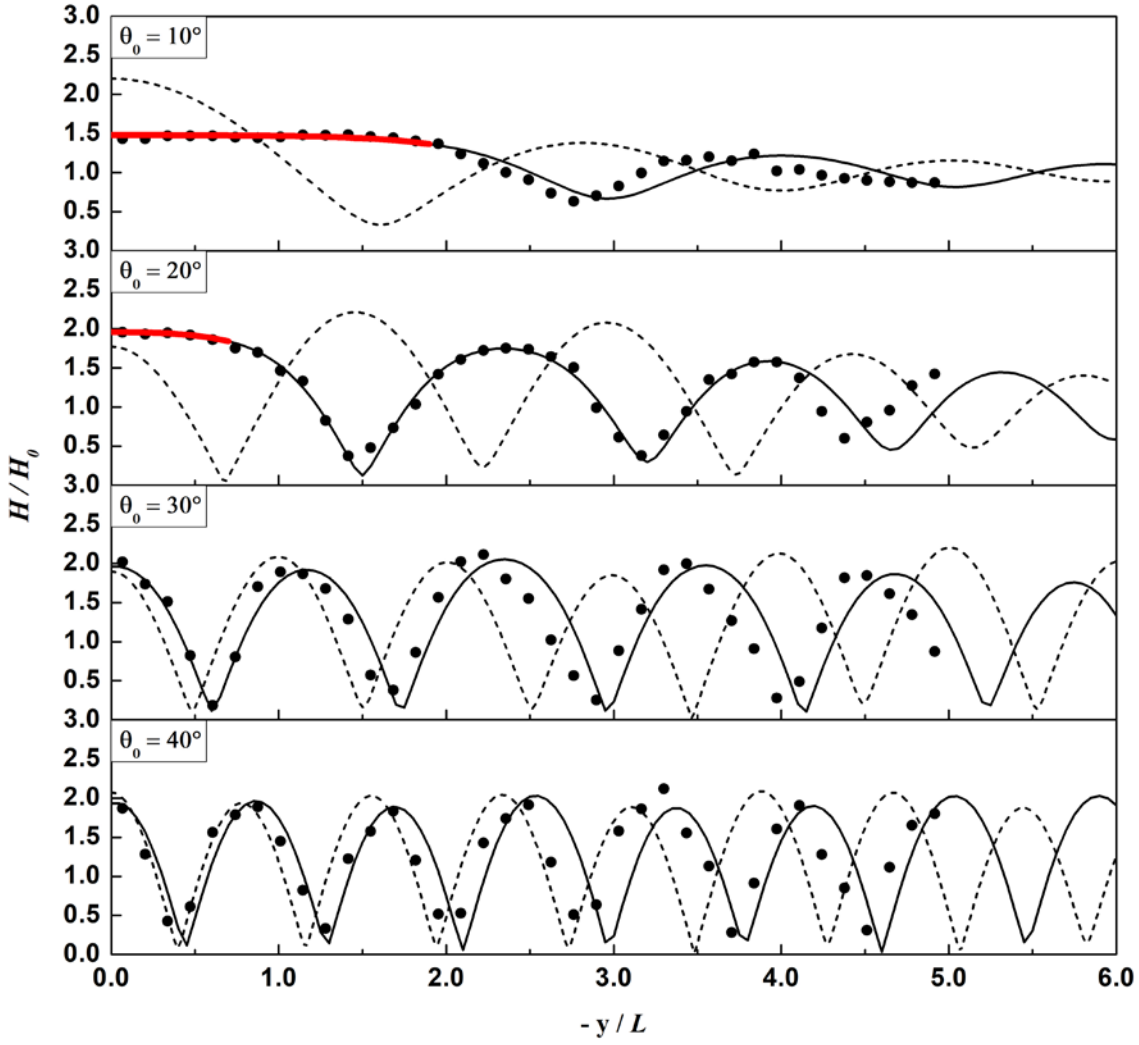

Figure 21. Normalized wave heights normal to the wall at x = 15L for the cases of MLL1 ~ MLL4. Solid circle (measured), solid line (present numerical), dashed line (analytical, Chen, 1987).

5

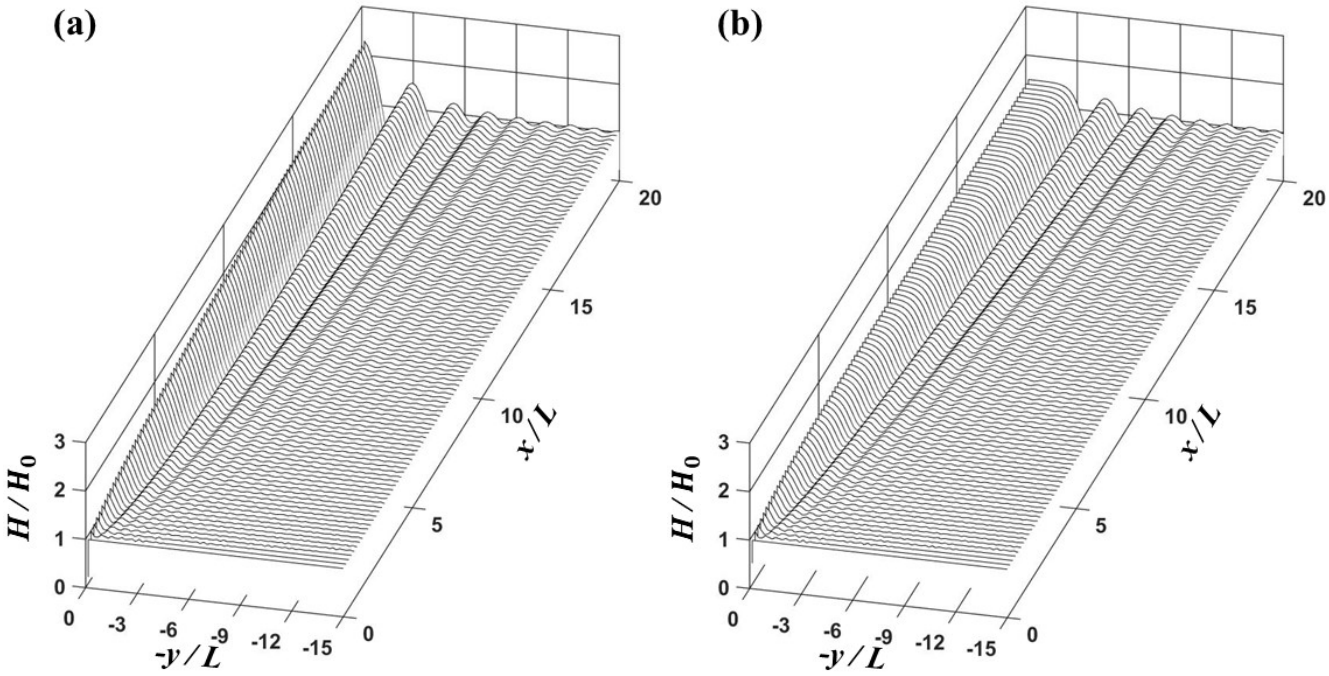

Figure 22. Three-dimensional plots of normalized wave height for (a) MLS1 and (b) MLL1 cases.

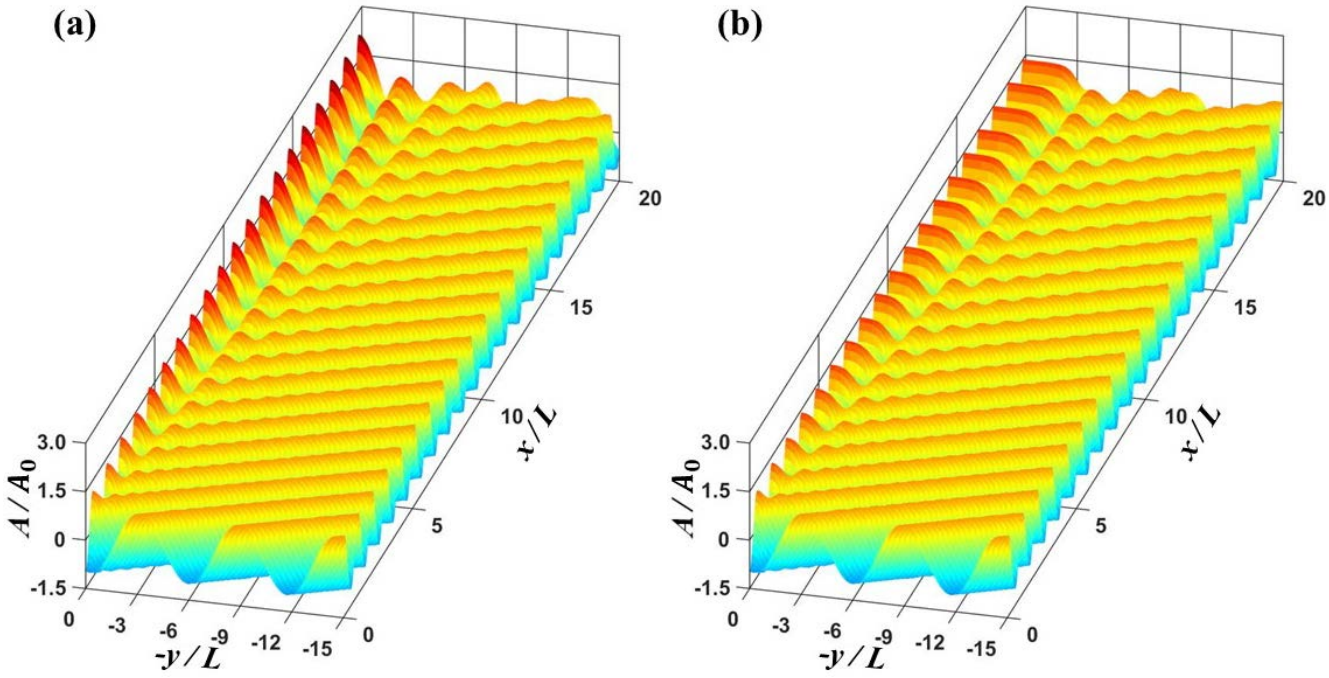

Figure 23. Three-dimensional plots of normalized free surface displacements (a) MLS1 and (b) MLL1 cases.

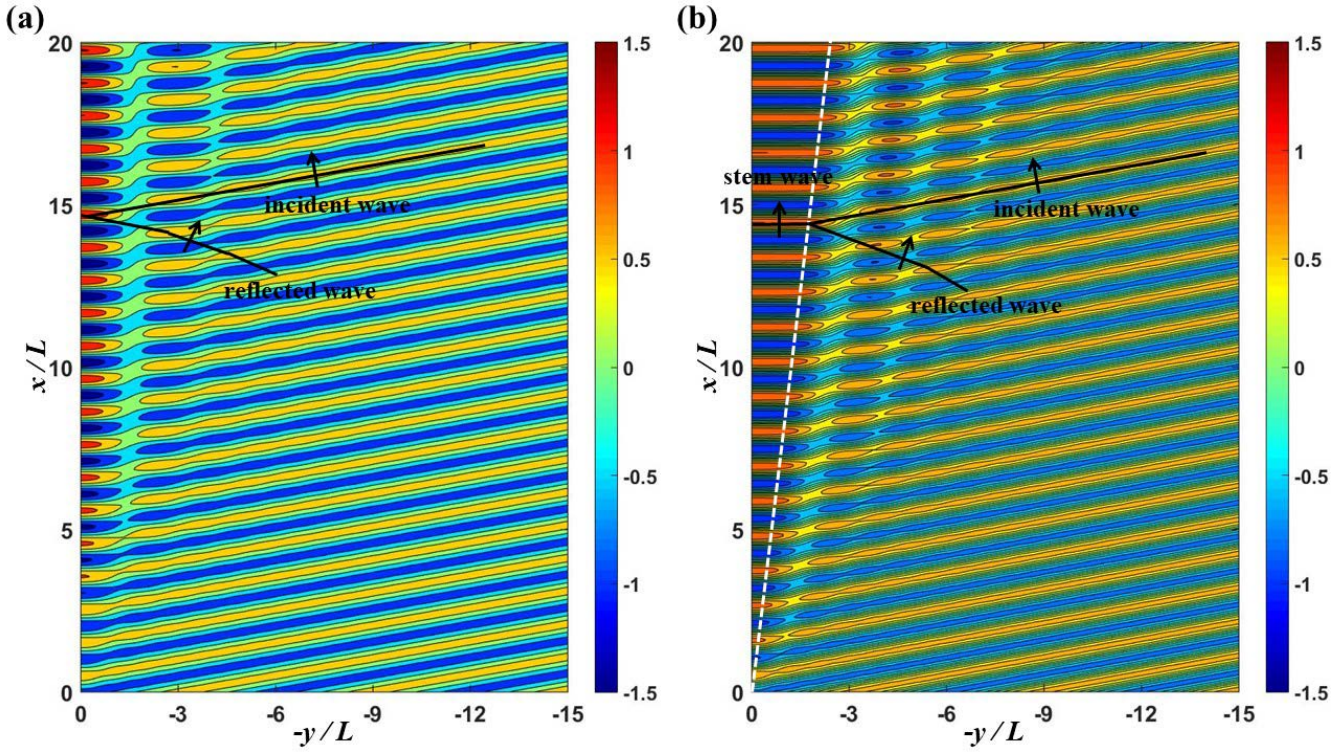

Figure 24. Contour plots of the instantaneous free surface for (a) MLS1 and (b) MLL1 cases.

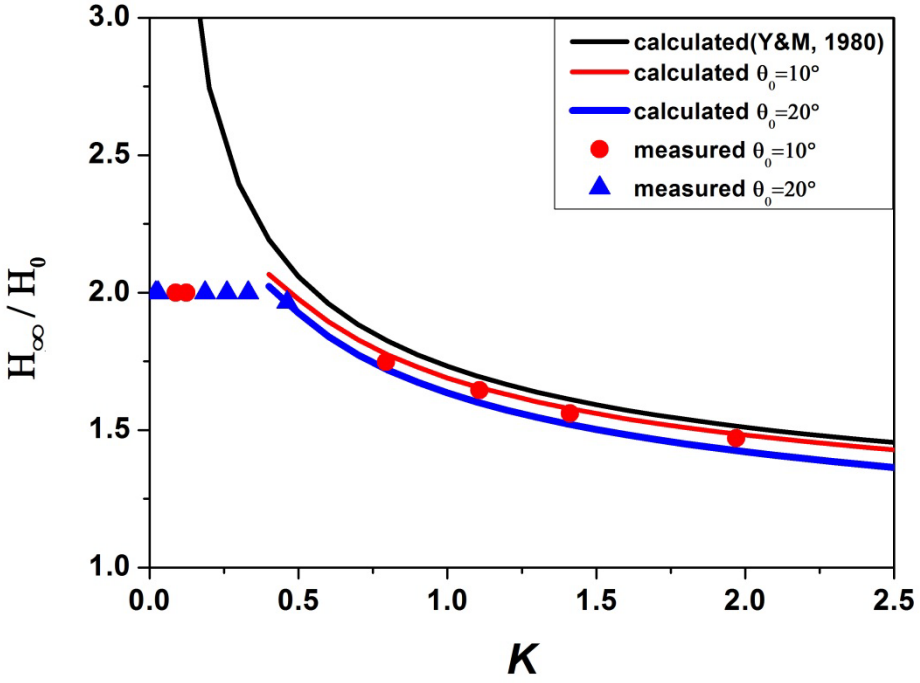

Figure 25. Comparison of calculated and measured normalized wave heights along the wall as a function of nonlinear parameter *K*. Black solid curve represents the wave height predicted by shock theory of Yue and Mei (1980), red and blue solid curves denote the calculated wave heights for $\theta_0 = 10°$ and $20°$, respectively. Symbols are measured data.

5

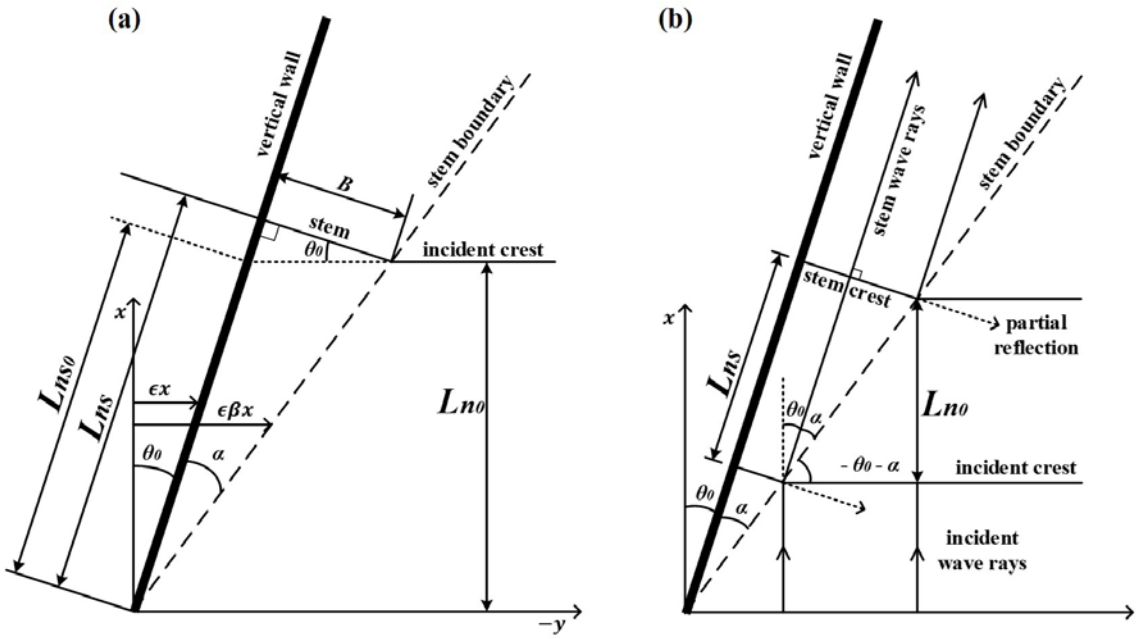

Figure 26. Definition sketch for geometrical relationship between incident and stem waves: (a) wave length approach, (b) wave ray approach.

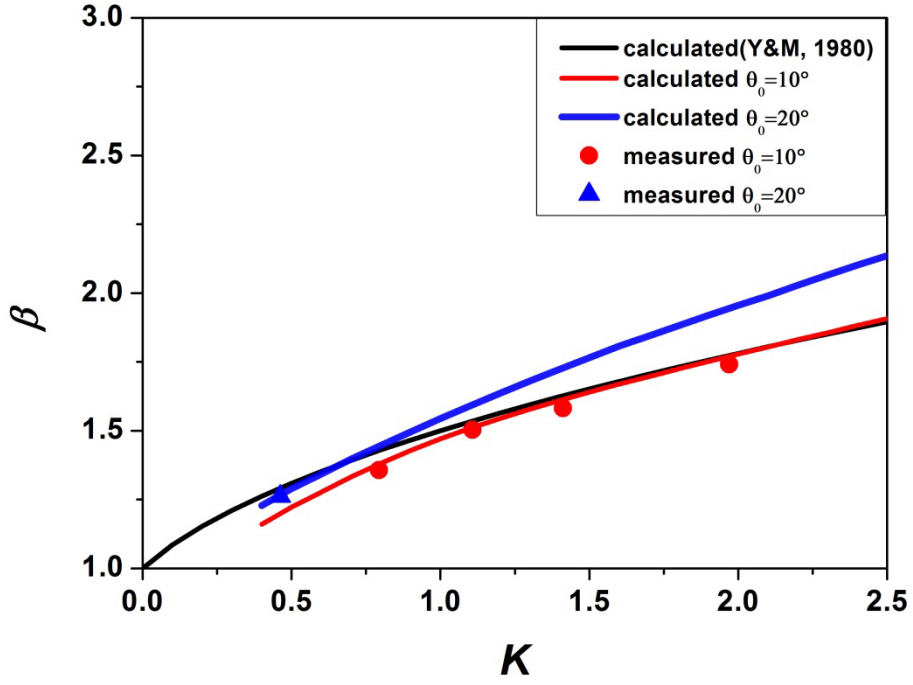

Figure 27. Comparison of calculated and measured β as a function of nonlinear parameter *K*. Black solid curve represents the calculated value using Yue and Mei (1980), red and blue solid curves denote the calculated values for $\theta_0 = 10°$ and $20°$, respectively. Symbols are measured data.

5

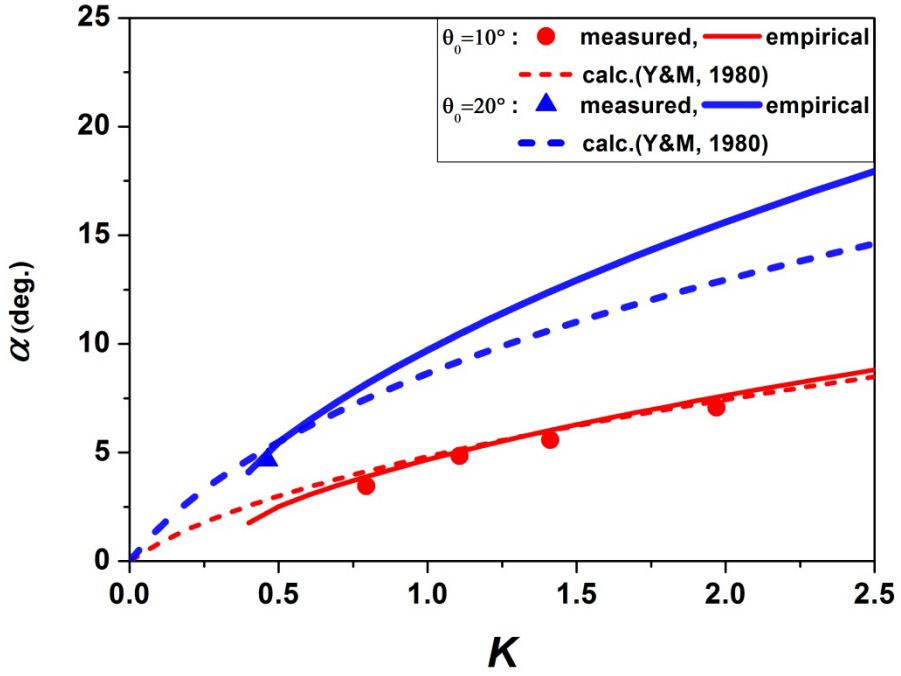

Figure 28. Comparison of calculated and measured stem angle α as a function of nonlinear parameter *K*. Dashed curves represent the calculated values using Yue and Mei (1980), solid curves are the calculated values using the present empirical formula, symbols are measured data. Red and blue colors are for $\theta_0 = 10°$ and 20°, respectively.

5